2002

# Transient thermomechanical interactions of shaft-bushing pair in bearings - a finite element study

Rajesh Krithivasan
*Louisiana State University and Agricultural and Mechanical College*, rkrith1@lsu.edu

# TRANSIENT THERMOMECHANICAL INTERACTIONS OF SHAFT-BUSHING PAIR IN BEARINGS – A FINITE ELEMENT STUDY

A Thesis

Submitted to the Graduate Faculty of the
Louisiana State University and
Agricultural and Mechanical College
in partial fulfillment of the
requirements for the degree of
Master of Science in Mechanical Engineering

in

The Department of Mechanical Engineering

by
Rajesh Krithivasan
B.E., PSG College of Technology, Bharathiyar University, 1997
December 2002

## ACKNOWLEDGEMENTS

I would like to express my gratitude to my advisor, Dr. Khonsari, for his invaluable guidance and encouragement throughout the course of this thesis work.

I am sincerely thankful to my committee members, Dr. Yitshak Ram and Dr. Wenjin Meng, for their support and spending their valuable time in evaluating my thesis work.

My special thanks goes to Mr. Haribabu Krishnamurthy for all the fruitful discussions we had that were instrumental for the successful completion of this thesis.

I also thank all my friends in the tribology group (CeRoM), for their moral and technical support, without which I would not have succeeded in finishing my thesis.

This work was supported in part by a grant from The Louisiana Board of Regents' Industrial Ties Research Subprogram with Caterpillar Inc (Grant # ITRS-007B-2002).

## TABLE OF CONTENTS

## NOMENCLATURE

| | | |
|---|---|---|
| $A_s$ | = | Area of the shaft that is in contact with the bushing, $m^2$ |
| $C$ | = | Radial clearance, m |
| $C_p$ | = | Specific heat capacity, J/kgK |
| $E$ | = | Young's modulus, $N/m^2$ |
| $f$ | = | Coefficient of friction |
| $h$ | = | Convective heat transfer coefficient, $W/m^2K$ |
| $k$ | = | Thermal conductivity, W/mK |
| $L$ | = | Length of the bearing in the normal direction, m |
| $N$ | = | Speed of the shaft, rpm |
| $n$ | = | Heat partition factor |
| $P$ | = | Contact force between the journal and the bearing, N |
| $q_s$ | = | Heat flux entering the shaft, $W/m^2$ |
| $Q$ | = | Heat generated, W |
| $R_{bi}$ | = | Inside radius of the bearing, m |
| $R_{bo}$ | = | Outer radius of the bearing, m |
| $R_s$ | = | Radius of the journal, m |
| $R_{eq}$ | = | Equivalent radius of contact, m |
| $T_\infty$ | = | Ambient temperature, $^\circ$C |
| $t_{ss}$ | = | Seizure time during start-up, seconds |
| $t_{sp}$ | = | Seizure time when lubricant flow disturbance occurs, seconds |
| $t_{fo}$ | = | Failure time for oscillating pin-bushing, seconds |

| | | |
|---|---|---|
| $\overline{t_{ss}}$ | = | Non-dimensional seizure time during start-up |
| $\overline{t_{sp}}$ | = | Non-dimensional seizure time during lubricant flow disturbance |
| $\overline{t_{fo}}$ | = | Non-dimensional failure time for oscillating pin-bushing |
| $t_{ref}$ | = | Transition time for the bearing to go from fully lubricated conditions to boundary lubrication conditions, seconds |
| $u$ | = | Surface velocity of the journal, m/s |
| $W$ | = | Load acting on the shaft, N |
| $\alpha$ | = | Coefficient of thermal expansion, m/mK |
| $\varepsilon$ | = | Non-dimensional thermal strain |
| $\kappa$ | = | Thermal diffusivity, $m^2/s$ |
| $\lambda$ | = | Non-dimensional modified aspect ratio |
| $\nu$ | = | Poisson's ratio |
| $\rho$ | = | Density of the material, $kg/m^3$ |
| $\theta_c$ | = | Contact angle, radians |
| $\tau$ | = | Frictional torque, Nm |
| $\omega$ | = | Angular velocity, radians/seconds |
| $\omega_o$ | = | Oscillating frequency, radians/seconds |

Subscripts

| | | |
|---|---|---|
| $s$ | = | Shaft or journal or pin |
| $b$ | = | Bearing |

## ABSTRACT

This thesis presents a finite element parametric study of the transient thermomechanical interactions of shaft-bushing pairs in bearings to gain insight into the nature of two categories of failures encountered in practice. The first type of failure deals with occurrence of the so-called thermally induced seizure (TIS) during the start-up period followed by an investigation of TIS due to a transient flow-disturbance. The second part deals with the thermomechanical interactions of pin-bushing assembly under heavy oscillating loads where the failure is by TIS and/or thermal galling. An extensive set of parametric simulations covering a wide range of loads, speeds, operating clearance, bearing dimensions, friction coefficients and thermal expansion coefficients are performed to gain insight into the phenomenon of TIS and thermal galling. A statistical procedure is applied to the simulated results and an appropriate empirical relationship is derived that predicts the time to failure for each category. Good agreement between the empirical and published results attests to the capability of the model and its potential for predicting bearing failure.

# CHAPTER 1. INTRODUCTION

The study of thermal effect on bearing performance has been considered to be an important subject since the evolution of tribology as a field of study. The driving force behind this is the frequent failure of tribological components due to metal-to-metal contact and the associated rise in the frictional heating. Thermally induced seizure and galling are examples of such failures relevant to this work. Thermally induced seizure occurs when the rise in operating temperature causes a partial or complete loss in operating clearance leading to the seizure of the journal in the bearing.

Galling failure, on the other hand refers to the condition whereby there is gross damage on the sliding surfaces characterized by the formation of local welding of surface.

The thesis concentrates on the transient thermomechanical interactions of journal and bearings under varying operating conditions encountered in practice. The research focused on the failure of journal bearings during start-up, failure of journal bearings during a transient flow disturbance, and the failure of a heavily loaded pin-bushing pair subject to oscillating heat fluxes.

## CHAPTER 2. LITERATURE REVIEW

Ling and Saibel [1] performed a study of failure of bearings due to thermal galling of sliding surfaces in contact. Galling was predicted to occur when the sliding surface reached the recrystallization temperature of the metal. The surface temperatures were calculated from Blok's criterion for predicting the flash temperature due to the asperity contact. Galling criteria was expressed as a function of the surface velocity, load and time. This criterion would be more appropriate for high energy sliding, like disc brakes and clutches. This work provided the author with the idea to use a similar failure criterion for bearings.

Dyson [2] presented a review of a type of failure and where gross damage characterized by the formation of local welding spots occurs between the sliding surfaces. This type of failure mode is sometimes referred to by technical terms like galling, scuffing and scoring. According to Dyson [2], "the metallurgical reaction on a scuffed or a galled surface is characterized by the formation of a hard, white, etch-resistant phase on the sliding surfaces. The identity of the phase is commonly thought to be a mixture of austenite, martensite and carbide. The presence of this transformed layer, often separated from the original untransformed bulk of the material by a tempered layer suggests that the scuffed surfaces have been subject to high temperatures and rapid cooling".

Gecim and Winer [3] performed a steady-state thermal analysis of a rotating cylinder subjected to heating in a particular region on its surface while the rest of the surface was subjected to convective cooling. The governing partial differential equation and boundary conditions were solved using the finite Fourier transform. The analogy between the analysis done by Gecim and Winer and a journal bearing undergoing

frictional heating is striking. A similar analysis was performed by Patula [4] to determine the steady state temperature of a rotating roller used in rolling of hot ingots in metal forming industry. Ulysee and Khonsari [5] generalized the conditions of a cylinder undergoing heating and cooling by including non-uniform heating and cooling. They obtained an analytical expression for the steady state solution using the Fourier transform method.

Bishop and Ettles [6] analyzed the thermoelastic interaction of a journal in a plastic bushing that was interference-fit with the shaft. The frictional heat generated was calculated as the product of the coefficient of friction, contact pressure and the sliding velocity. Bearing seizure was considered to have occurred when the temperature rise on the surface of the shaft exceeded $360^{o}$C. In that study, the shaft was considered to expand radially outwards due to the rise in temperature. The expansion of the bushing was ignored, as the temperature rise is not appreciable as the thermal conductivity of plastic was low. Bishop and Ettles considered the temperature rise to be dependent primarily on the load, speed and clearance and arrived at a critical PV/C number as a bearing seizure number.

Dufrane and Kannel [7] performed a study of the thermoelastic interactions of a journal bearing undergoing a catastrophic seizure leading to a complete loss in operating clearance. The cause of this type of failure was identified to be dry metal-to-metal contact during the bearing start-up and associated rise in the contact temperature. Bearings that had been out of service for a relatively long time are particularly susceptible because of the lack of adequate supply of the lubricant in the contact area. The work is of particular importance as the encroachment of the shaft to the bushing and the concomitant reduction

in the operating clearance (on the order of microns) was found to occur rapidly. Dufrane and Kannel performed a series of experiments to determine the effect of dry friction that led to failure by seizure. The experimental results showed that typically seizure occurred within 30 seconds in most journal bearings operating in dry conditions. A one-dimensional thermal and thermoelastic analysis was performed to estimate the seizure time as a function of the operating parameters. The shaft expanded radially outward and seizure was assumed to be complete when the total operating clearance vanished. The bearing thermal expansion was not considered in the theoretical analysis. A linear analytical expression was derived relating the bearing operating conditions and the seizure time. This linear equation holds good only for very short transient times. Although it gave good results that matched experiments, it is somewhat restrictive and does not accurately represent the behavior of the system. The linear variation of seizure time with clearance implies that all bearings irrespective of the operating clearance would eventually seize.

Khonsari and Kim [8], inspired by the work done by Dufrane and Kannel, performed a 2-D finite element analysis to study the thermoelastic behavior of journal bearings undergoing seizure during start-up. They developed two models, one with an aligned journal and bearing and the other with an axial misalignment. The 2-D axial model included the effect of heat transfer in the axial direction. A heat-partitioning factor was calculated based on the ratio of the areas of contact of the journal and the bearing. The results proved that the seizure time tended to "flatten out" with increasing time. This non-linear expression closely captures the physics of the reduction in clearance with time. If a misalignment were present in the axial direction, the shaft comes into contact with

the bearing on a very small area, further aggravating the thermomechanical interaction. Khonsari and Kim approximated this as a point heat source and presented results reveled that the misalignment of the journal in the axial direction led to faster seizure times.

Hazlett and Khonsari [9, 10] continued the research to gain further understanding of the behavior of a journal bearing undergoing seizure. They developed a thermomechanical finite element model using the finite element package ANSYS. The thermal analysis was first done to study the effects of the frictional heating on the contact area of the bushing and the entire area of the shaft. The thermal analysis incorporated the partition of frictional heat generated at the contact area based on the ratio of the areas of contact of the journal and the bearing. The thermal contact resistance at the contact area between the shaft and the bushing was modeled using convection link elements. The results of the thermal analysis were used as thermal loads for solving the thermoelastic model. The operating clearance was modeled by contact elements available in the ANSYS element library. These elements come into effect only when there is a contact between the journal and the bearing. The status of these elements was used to find the variation of clearance and contact forces over time. Frictional torque was introduced as the basis for seizure. When the frictional exceeded a limiting value, the bearing is assumed to be seized. Based on the results of the thermomechanical analysis, Hazlett and Khonsari found that the encroachment of the shaft into the bearing was non-linear with time. The results established that TIS is triggered by the ovalization of the bushing and formation of new contact patches at the top of the bearing. The establishment of new contact patches accelerated the seizure process by increasing the contact forces and thus

increasing the frictional torque. This may be visualized as a positive feedback of thermal energy into the system accelerating the process of seizure.

Wang, Conry and Cusano [11,12] performed a finite element study of the burn-off and force stack-up in a railroad axle. An axially symmetric finite element and a radially symmetric finite element analyses were performed simultaneously to simulate the 3D analysis. The thermal analysis was similar to the analysis procedure performed by Hazlett and Khonsari. The partition of heat between the journal and the bearing was done by iteratively comparing the surface temperatures of the radial and axisymmetric models. This model of heat partitioning was found to match closely with the results of the partitioning method used by Hazlett and Khonsari. Radiation was also considered in the thermal analysis. This is of importance as the temperature rise in the journal-bearing system was very large. Temperature dependent material properties and friction coefficients were used because of the high temperatures involved. Failure of the railroad followed two patterns depending on the clearances involved. When the clearances are low (0.05 mm - 0.5 mm), the failure was due to seizure of the axle in the bearing cone. The seizure patterns were similar to those reported by Hazlett and Khonsari. New contact areas were established that triggered seizure. When the clearances are sufficiently large (2 mm – 5 mm), the failure was due to axle burn-off. The bearings operated for a long time subjected to frictional heating continuously and the temperatures reached recrystallization temperatures when the failure happened due to axle burn-off at high temperatures.

More recently, Wang [13] performed a review of published results on TIS in conformal contacts. It revealed that seizure in unlubricated conformal contacts was

primarily due to a thermal ratcheting effect in a positive feedback of increases of interfacial pressure and heat. In lubricated journal bearings, starvation of the oil was found to be a direct cause for seizure. The starvation led to wear and temperature rise in the contact area that caused the onset of seizure. Other factors that affect the seizure process are the surface quality and chemical composition, surface roughness and microstructure of the shaft and the bushing.

Thermally induced Seizure (TIS) can also occur in circumstances where there is a disturbance in the steady-state operation of the journal bearing. Lacey and Kawamura [14] performed a study on the effects of lubricant flow disturbance in aircraft gas turbine engine bearings. These bearings are required to survive with little or no oil under severe operating conditions such as those encountered during flight take-off, landing and sudden maneuvering. The oil flow interruption typically lasts for 15 to 30 seconds. The aircraft engine bearings are not only required to survive these operating conditions but also to resume normal operation once the lubricant flow is re-established. Although this study was done to improve the performance of ball bearings in aircraft engines, the inspiration to perform a similar study on journal bearings was developed. The effects of the oil flow interruption in lubricant supply took place in either of the two mechanisms described below:

(1) Oil flow interruption $\Rightarrow$ Adverse $\Delta T$ $\Rightarrow$ Reduction in bearing clearance $\Rightarrow$ Excessive Hertzian stresses $\Rightarrow$ High heat generation $\Rightarrow$ Bearing seizure.

(2) Oil flow interruption $\Rightarrow$ Surface damage (Wear) $\Rightarrow$ High heat generation $\Rightarrow$ Reduction in bearing clearance $\Rightarrow$ Seizure.

This study provided the author the inspiration to study the effects of flow disturbance in journal bearings that may occur due to supply line blockage, contaminant blockage, airlock etc.

Thermally induced seizure is not a phenomenon restricted to bearings operating under dry or boundary lubricated conditions. It can also occur in bearings running in fully lubricated condition. This phenomenon was discussed by Pascovici, Khonsari and Jang [15] and an analytical model was formulated for this transient analysis. Performing an energy balance on a lumped system, the thermal response of the journal bearing is obtained. A limiting temperature is taken as the condition for onset of seizure. This limiting temperature is when the clearance between the journal and the bearing is completely lost. A "no-seizure" condition is also derived based on the limiting temperature.

Jang, Khonsari and Pascovici [16] performed a comprehensive analytical and experimental study on the thermohydrodynamic (THD) seizure in journal bearings. The experimental set-up studied THD seizure in an unloaded bearing that is operating in fully lubricated conditions. The journal was made of polyamide and the bearing was made of glass-reinforced epoxy resin. The seizure time was determined when the driving torque requirement exceeded a certain range. A theoretical THD analysis was done to determine the thermal response of the lubricating oil. The viscous dissipation caused the oil temperature to rise. The thermal expansion of the shaft and its encroachment into the bushing was determined using a standard 2-D heat conduction equation. The boundary conditions at the interface of the shaft and the fluid film were determined from the THD analysis. Good agreement of theoretical and experimental seizure time was observed.

## CHAPTER 3. FINITE ELEMENT ANALYSIS: PROCEDURE AND OVERVIEW

The objective of this thesis is to study the thermomechanical interactions of journal-nearing systems subject to different types of boundary conditions like unlubricated bearing start-up, a fully-lubricated bearing undergoing a disturbance in the lubricant oil supply and a journal and bearing subject to oscillating heating. The finite element analysis is a simple and handy tool that is used with good accuracy in engineering. The commercial FEM software package ANSYS 5.7 was utilized to perform a detailed analysis of the thermoelastic interactions of journal and bearing. In this chapter, the finite element analysis procedure, the type of elements used and the boundary conditions involved are presented with the theoretical background [17, 18, and 19].

### 3.1 Thermal Analysis – Theory and Finite Element Formulation

Heat conduction analysis must be performed to determine the material temperatures and the heat flow rates. The temperature distribution is also needed in order to perform an analysis for thermally induced stresses. Fortunately, it is possible to devise a single mesh layout for both problems: a computer program can read a single data file, compute the temperatures at the nodes, then use these temperatures in a thermomechanical analysis to compute the displacement, stresses etc.

For an isotropic material with no internal heat generation, Equation 3.1 and 3.2 give the governing equation for heat conduction under transient condition in rectangular and polar coordinates respectively [18].

$$k\frac{\partial^2\theta}{\partial x^2}+k\frac{\partial^2\theta}{\partial y^2}=\frac{\rho\, C_p}{k}\frac{\partial\theta}{\partial t} \tag{3.1}$$

$$\frac{\partial^2\theta}{\partial r^2}+\frac{1}{r}\frac{\partial\theta}{\partial r}+\frac{\partial^2\theta}{\partial\varphi^2}=\frac{\rho\, C_p}{k}\frac{\partial\theta}{\partial t} \tag{3.2}$$

where $\theta$ = Rise in temperature, $^{o}$C

$k$ = thermal conductivity of the material, W/mK

$\rho$ = Density of the material, kg/m$^3$

$C_p$= Specific heat capacity of the material, J/kgK

$t$ = time, seconds

Equation 3.1 and 3.2 can be solved analytically if we know the geometry of the solid and its material properties and four boundary conditions (2 in the *x/r*-direction and 2 in the *y/ϕ*-direction) and one initial condition. There are normally two types of boundary conditions to solve a thermal analysis: (i) the Dirichlet boundary condition, where the temperature boundary conditions are specified and (ii) the Neumann boundary conditions, where the surface boundary conditions like heat flux or convection are specified.

Equation 3.3 gives the equivalent finite element formulation for the transient thermal analysis. Note that Equation 3.3 is the formulation for a single element [17]. The elements are arranged in a global matrix formulation to arrive at the complete solution. The finite element formulation does not depend on the coordinate system.

$$([k]+[H])\{T\}+[C]\left\{\frac{\partial T}{\partial t}\right\}=\{R_q\}+\{R_h\} \tag{3.3}$$

where $[k]$ = element thermal stiffness matrix = $\int_{V_e}[B]^T[\mathrm{K}][B]dV$

$[H] \quad = \int_{S_e}[N]^T[h][N]dS$

$[C] = \int_{V_e} [N]^T \rho\, C_P [N] dV$

$\{R_q\} = \int_{S_e} [N]^T q_b\, dS$ , Boundary condition matrix on surface, $S_e$

$\{R_h\} = \int_{S_e} [N]^T hT_f\, dS$ , Boundary condition matrix on surface, $S_e$

[K] = Thermal conductivity matrix of the material

[*N*] is the shape function of the element used in the finite element analysis. [*B*] is the strain displacement matrix, which is a spatial derivative of the shape function matrix, [*N*]. The shape function of a finite element is defined as the interpolation function that describes the distribution of the degree of freedom (temperature, displacements etc.) across the element. Four-noded elements as shown in Figure 3.1 were used in the analyses in this thesis for modeling thermal solids. The temperature field across the element is modeled as a linear function of the nodal temperatures. For such a 4-noded element, the shape function matrix and the strain displacement matrix are given by the following equations 3.4 and 3.5.

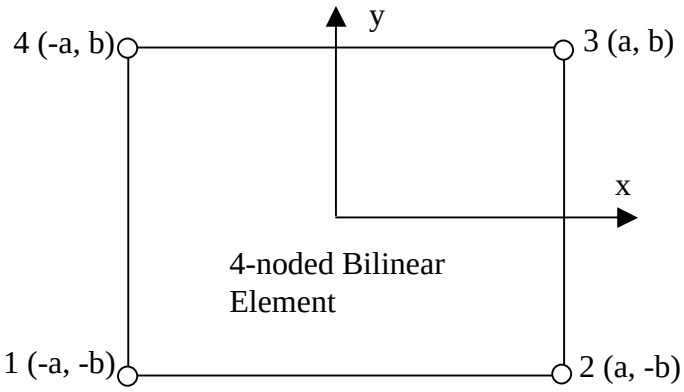


Figure 3.1 – 4-noded bilinear element

$$[N] = \left\{ \frac{(a-x)(b-y)}{4ab}, \frac{(a+x)(b-y)}{4ab}, \frac{(a+x)(b+y)}{4ab}, \frac{(a-x)(b+y)}{4ab} \right\} \qquad (3.4)$$

$$[B] = \begin{bmatrix} \partial/\partial x & 0 \\ 0 & \partial/\partial y \\ \partial/\partial y & \partial/\partial x \end{bmatrix} [N] \tag{3.5}$$

The shape functions in finite element packages like ANSYS have a robust solver that can solve for elements that are not necessarily a regular rectangular shape. A parametric formulation effectively solves for complex geometries. The shape functions are modified accordingly but the bilinearity is maintained. If $T_1$, $T_2$, $T_3$ and $T_4$ are the nodal temperatures of the element shown in Figure 3.1, then the temperature field across the element is given by:

$$T(x, y) = \frac{(a-x)(b-y)}{4ab} T_1 + \frac{(a+x)(b-y)}{4ab} T_2 + \frac{(a+x)(b+y)}{4ab} T_3 + \frac{(a-x)(b+y)}{4ab} T_4$$

**3.2 Thermoelastic Analysis – Theory and Finite Element Formulation**

The thermoelastic analysis is done to determine the displacements at nodes, stresses, strains, etc. The results of the thermal analysis are input as nodal loads to determine the temperature effects on the elastic behavior. Stress on an element can be calculated when its nodal degrees of freedom (d.o.f.s) are known. These nodal d.o.f.s are available after the structural governing equation (3.6) has been solved [17].

$$[K]\{D\}=\{R\} \tag{3.6}$$

where $[K]$ = Structural stiffness matrix of the bilinear element, as shown in Fig 3.1

$$= \int_{-b}^{b} \int_{-a}^{a} [B]^T [E][B] t \, dxdy$$

$\{D\}$ = Nodal displacement matrix.

$\{R\}$ = Load matrix.

$[E]$ = Young's modulus matrix = $\begin{bmatrix} E & 0 & 0 \\ 0 & E & 0 \\ 0 & 0 & E \end{bmatrix}$, for isotropic materials

The stresses in a finite element can be solved from the solution of Equation 3.6 and imposing the temperatures as nodal loads acting at the nodes. The temperature at nodes is found by performing a thermal analysis that is solved before running the thermomechanical analysis. If the nodal temperatures of an element is given by the following matrix.

$$\{T_e\} = [T_1, T_2, T_3, T_4]^T$$

then the thermal nodal loads for solving the thermomechanical analysis are given by the following matrix [17].

Thermal Load Matrix: $\{R_e\} = \varepsilon A_e \alpha [T_1, T_2, T_3, T_4]^T$

Equation 3.7 and 3.8 are used to solve for the stresses in plane stress conditions and plane strain conditions respectively.

For a general case, the generalized Hooke's law is given by the following equation:

$$\{\sigma\} = [E](\{\varepsilon\} - \{\varepsilon_0\})$$

where $\{\varepsilon_0\}$ represents the strains due to the thermal expansion caused by the nodal loads exported from the thermal analysis.

The stress field for plane stress problems is given by Equation 3.7 [17].

$$\begin{Bmatrix} \sigma_x \\ \sigma_y \\ \tau_{yx} \end{Bmatrix} = \frac{E}{1-\nu^2} \begin{bmatrix} 1 & \nu & 0 \\ \nu & 1 & 0 \\ 0 & 0 & \frac{1-\nu}{2} \end{bmatrix} \left( [B]\{D\} - \begin{Bmatrix} \alpha T \\ \alpha T \\ 0 \end{Bmatrix} \right) \tag{3.7}$$

The stress field for plane strain problems is given by Equation 3.8 [17].

$$\begin{Bmatrix}\sigma_x\\ \sigma_y\\ \tau_{yx}\end{Bmatrix} = \frac{E}{(1-2\nu)(1+\nu)}\begin{bmatrix}1-\nu & \nu & 0\\ \nu & 1-\nu & 0\\ 0 & 0 & \frac{1-2\nu}{2}\end{bmatrix}\left([B]\{D\} - \begin{Bmatrix}\alpha T\\ \alpha T\\ 0\end{Bmatrix}\right) \tag{3.8}$$

The specific boundary conditions, element types and loading for the various analyses are described in brief in Sections 4, 5 and 6 as per the specific problem.

## CHAPTER 4. THERMALLY INDUCED SEIZURE IN JOURNAL BEARINGS DURING START UP

Thermally induced seizure (TIS) in journal bearings is a mode of failure that can occur quite suddenly and end up with a catastrophic damage to the system. Although TIS can take place in lubricated bearings, it is predominant when a hydrodynamic bearing happens to operate in the boundary or mixed lubrication regimes. These conditions occur during start-up or in an event of lubricant supply blockage.

A significant amount of work has been reported that analyzed the thermomechanical interactions in stationary loaded bearings susceptible to TIS. Bishop and Ettles [6] analyzed the thermoelastic interaction of a journal in a plastic bushing that is interference-fit with the shaft. The seizure criterion was based on a cut-off temperature. When the surface temperature of the shaft or the bushing reaches $320^{o}$ above the ambient temperature, the shaft is assumed to seize in the bearing. A critical *PV/C* number was proposed to be an influential parameter for assessing the seizure time. Dufrane and Kannel [7] analyzed the catastrophic seizure of bearings due to dry friction by a simple 1D equation relating the seizure time to the bearing operating parameters and material properties. A series of experiments were also conducted to determine the seizure time

$$t_{ss} = \frac{C\rho C_p}{2(1+\nu)\alpha q_s} \bullet \frac{1}{\left[(n-1)\left(R_{bo}/R_s - R_s/R_{bo}\right)^{-1} + n\right]} \tag{4.1}$$

Equation (4.1) predicts a linear relation between the seizure time and the operating clearance. This means that the bearing will seize even if the clearance is very large. Khonsari and Kim [8] performed a comprehensive 2D numerical analysis of a bearing undergoing seizure during start-up. The analysis included axial length of the

bearing as well as the effects of a misaligned shaft on the thermoelastic interactions. This study established a non-linear nature for the clearance loss as a function of time. Hazlett and Khonsari [9,10] performed a detailed finite element analysis to gain insight into the nature of the contact forces and encroachment of the mating pair leading to TIS of a dry bearing during start up. Their analysis revealed that the thermoelastic deformation between the journal and the bearing led to a reduction in clearance in a non-linear fashion. The effect of bearing parameters on the seizure time was also performed as a sensitivity study. More recently, Wang et.al. [11,12] analyzed the axle burn-off and stack-up force of a railroad roller bearing using the finite element method and independently verified the results of Hazlett and Khonsari's findings. More recently, Wang [13] performed a review of published results on TIS in conformal contacts. It revealed that seizure in unlubricated conformal contacts was primarily due to a thermal ratcheting effect in a positive feedback of increases of interfacial pressure and heat. In lubricated journal bearings, starvation of the oil was found to be a direct cause for seizure. The starvation led to wear and temperature rise in the contact area that caused the onset of seizure. Other factors that affect the seizure process are the surface quality and chemical composition, surface roughness and microstructure of the shaft and the bushing.

The objective of this work is to perform a comprehensive study of seizure in bearings during start-up and arrive at a seizure time evaluation formula that is a function of the various operating parameters. The aim of the work is to provide a simple empirical relation for practicing engineers and lubrication system designers to predict the seizure time, which can help them to design instrumentation systems and warning devices to take necessary precautions.

## 4.1 Finite Element Modeling Procedure

The finite element modeling is done using ANSYS 5.7. [19] First, the analysis done by Hazlett [9,10] was recreated. The finite element model of the present work employs a finer mesh than the mesh used by Hazlett and Khonsari to evaluate the contact forces with more accuracy. A simplified 2-dimensional analysis is performed. The analysis assumes that the contact pressure is uniform in the axial direction and no crowning or misalignment is present in the system. The effect of bearing length is analyzed in the 2-D analysis by taking into account the change in the contact width and change in the heat flux generated with change in bearing length.

The analysis of a bearing undergoing TIS during start up is done by the following steps:

1. A 2-D static contact analysis was performed to determine the contact forces and the contact angle.
2. A transient heat transfer analysis was done to model thermal effects of dry frictional heating on the journal and the bearing.
3. A transient thermoelastic analysis was performed to study the interactions of the journal-bearing pair during bearing start-up. The variation of radial clearance, contact forces and ovalization of the bearing were studied in this analysis.

**Analysis Model**

The model consists of a shaft rubbing on the inner surface of the bushing as shown in Figure 4.1. The contact forces results in the generation of frictional heat on the entire surface of the shaft and in the area where it contacts the bushing inner radius. Due to the rise in temperature, the shaft expands and its encroachment to the bushing leads to

a loss of clearance. At some point in time, the bearing clearance reduces to a minimum and shaft starts to encroach the bearing. Analyses show that typically during TIS, the following three phenomena occur: (i) The contact forces increase, increasing the heat generated. (ii) The contact angle increases causing a higher percentage of heat entering the bush. (iii) New areas of contacts are established resulting in a chain reaction of events leading to a rapid loss in the operating clearance. In the simulations presented in this paper, these processes were implemented by performing a thermal analysis and a thermoelastic analysis in a stepwise linear fashion. The model utilized a one-half symmetry and neglected the heat conduction in the axial direction.

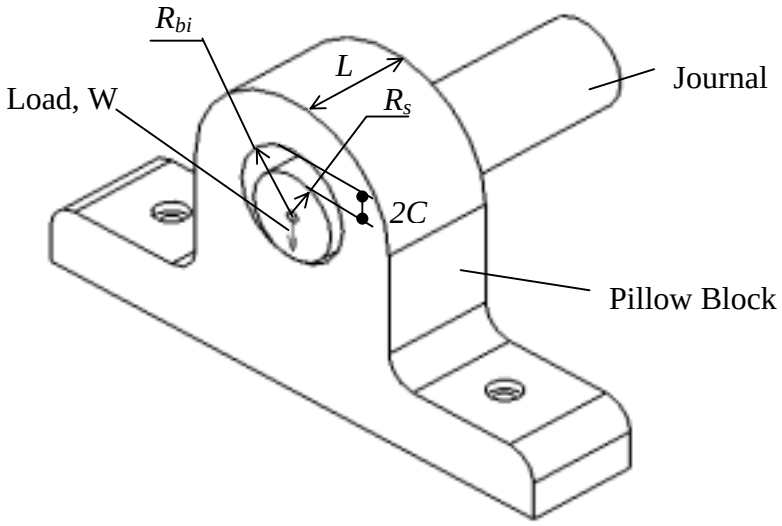


Figure 4.1 – Schematic of a journal supported on a pillow block

### 4.1.1 Transient Thermal Finite Element Analysis

**Thermal Elements** - The thermal analysis is done to determine the temperature distribution in the journal-bushing pair. The journal and bushing were modeled as 4-noded solid thermal elements viz. PLANE55. PLANE55 element has a single degree of

freedom, namely temperature. This element is compatible with the 4-noded structural solid element used in the thermomechanical analysis. This means that the results of the thermal analysis can be successfully exported to perform the thermoelastic analysis

**Loading -** The loading applied in the thermal analysis consists of the heat generated by the frictional contact at the shaft-bushing interface. The total heat generated in the contact zone is:

$$Q = fu\sum_{i=1}^{n} P_i \tag{4.2}$$

where $f$ is the coefficient of friction of the rubbing surfaces, $\sum P_i$ is the summation of the contact forces; $n$ the total number of elements in contact and $u$ is the surface velocity of the shaft. The summation of the contact forces was equal to the total load acting on the system, $W$. The frictional heat generated heats the entire surface area of the shaft in an on-off mode. Thus the surface of the shaft is intermittently heated in the contact area and cooled in the clearance area. The frictional heat generated heats only the surface of the bushing that is in contact. Temperature and flux continuity exists in the contact patch of contact of the journal and the bearing. The heat flux due to the frictional heating is computed using the following formulae.

$$q_s = \frac{f.u.\sum P_i}{A_s} = \frac{f.u.\sum P_i}{2\pi R_s L} \tag{4.3}$$

**Boundary Conditions -** The rotating shaft is heated periodically when it makes contact with the bushing. This can be thought of as an on-off type heating. It was shown by Hazlett [10] that the on-off heating could be modeled as an average heat flux on the entire surface. Also, there is dissipation of heat by convective cooling by the air within the clearance of the journal and the bushing

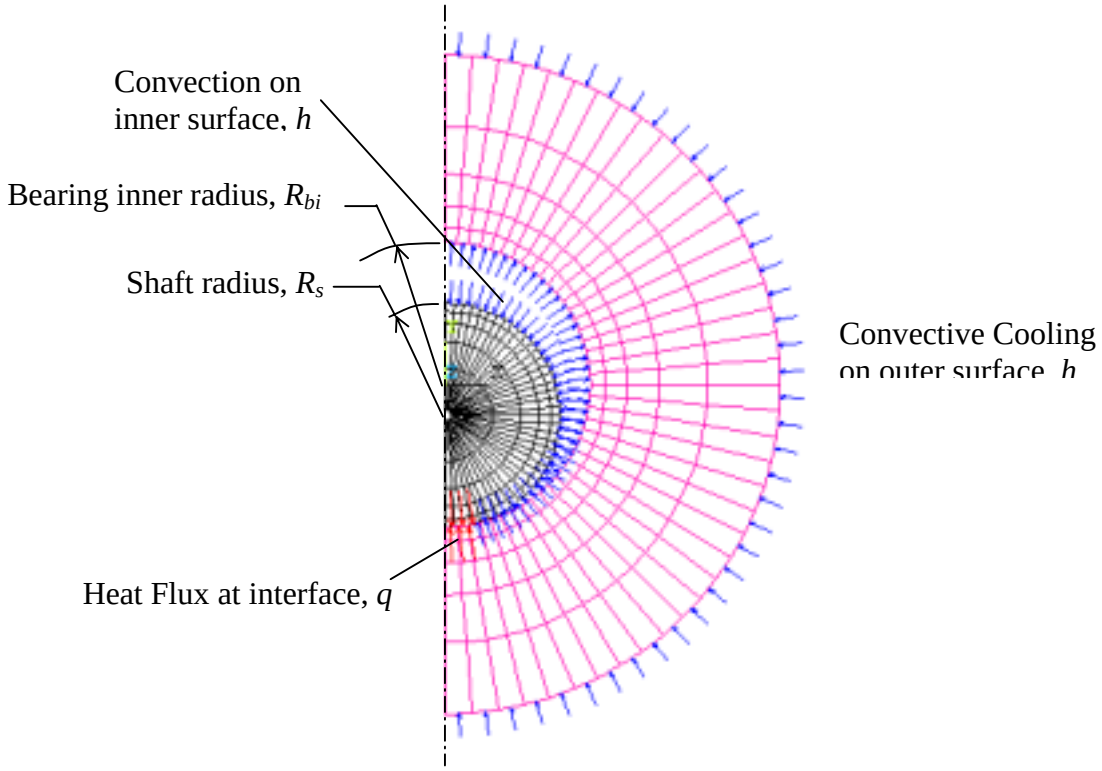


Figure 4.2 - Finite Element Model for Thermal Analysis, with loads and boundary conditions. (Not to scale)

To represent the periodic heat dissipation in the finite element model, the nodes on the surface of the shaft are coupled. The temperature on the surface of the journal and the bushing at the interface is constant and is modeled by coupling the temperatures at the nodes on the interface. The outer surface of the bushing is subject to natural convection. The finite element mesh, thermal boundary conditions and the thermal loads are schematically represented in Figure 4.2. For clarity, the operating clearance in Figure 4.2 is scaled by a factor of approximately 300.

### 4.1.2 Non-linear Transient Elastic Finite Element Model

**Elastic/Thermoelastic Elements -** The steady state analysis to find the contact forces and the transient thermoelastic analysis use two types of elements in the Finite Element Program ANSYS 5.7. The solid element PLANE42 is used to model the journal

and the bush. This element is a 2D bilinear element with the displacements in the x and y directions as the degrees of freedom. The radial clearance between the journal and the bush is modeled using two-noded contact elements, namely CONTAC52. Contact elements are used to model gap and they come into effect only when the two nodes that make the element come into contact. The element properties include a normal stiffness value that governs the resistance to normal load. The finite element programmer assigns the stiffness value for the contact element. To find the stiffness value, the theoretical Hertzian contact width [20] must be determined. The stiffness value is then fixed at a value by trial and error so that the Hertzian contact width and the contact width found by Finite Element method are the same. The ANSYS 5.7 manual suggests that the normal stiffness value for the contact element CONTAC52 can vary in the range of 0.01 to 100 times the stiffness of the underlying solid element material. The manual also suggests the programmer to use his judgment in the trial and error method used to finalize the stiffness value. The verification of the stiffness value against the Hertzian theory [20] was followed to establish validity.

**Loading -** The loading for the non-linear thermoelastic analysis consists of the thermal loads applied as nodal temperatures and the radial force acting on the journal. The time dependent thermal load is obtained from the results of the transient thermal analysis. The static load, W is applied to act in the negative y-direction on the shaft. As the model utilizes half-symmetry, a load of W/2 is applied.

**Boundary Conditions -** Symmetry boundary conditions are used to model the one-half symmetry as shown in Figure 4.3. The constraint of the bearing on its outer surface is modeled by fixing the bearing at the node under the shaft on the outer edge of

the bearing on the symmetry plane. This constraint approximates the boundary conditions that could be expected from a pillow block type of bearing as shown in Figures 4.1 and 4.3.

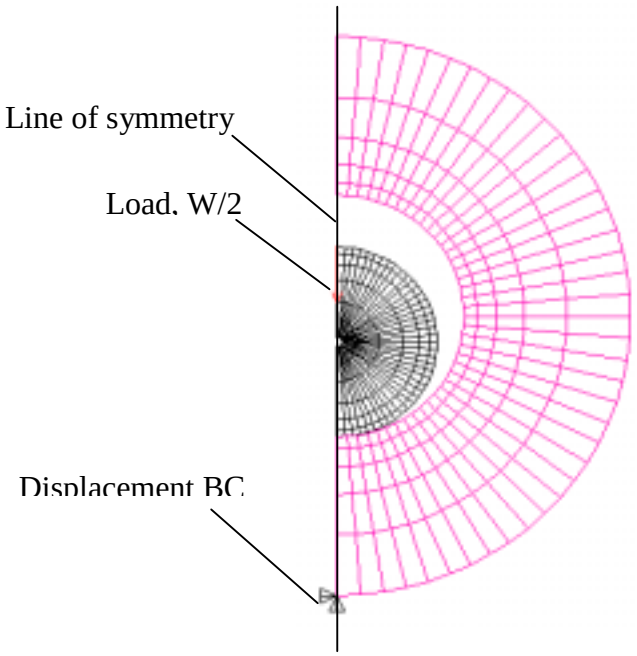


Figure 4.3 - ANSYS Model for Elastic Analysis, with loads and boundary conditions

### 4.1.3 Seizure Criterion

Frictional torque is the torque resisting the driving torque exerted by the motor. When the frictional torque increases beyond the extent of the driving torque capability, it can be concluded that the journal has seized in the bearing. The present model assumes that TIS is complete when the frictional torque reaches at least 50 times the driving torque. The contact forces acting on the gap elements at any instant of time determine the frictional torque at any time.

$$\tau(t) = 2.f.R_s.\sum_{i=1}^{m} P_i(t) \qquad (4.4)$$

where T is the frictional torque, $f$ is the coefficient of friction, $R_s$ is the radius of the shaft and $P_i$ is the contact force at the $i$'th gap element and $n$ is the number of elements in contact.

**4.2 Results and Discussion**

The encroachment of the shaft on to the bushing with concomitant reduction in the clearance continues until the seizure is complete. The process is a complex, non-linear phenomenon. Analysis shows that TIS is initiated by the ovalization of the bearing combined with the uniform outward expansion of the shaft yielding contact between the top of the shaft and the inner bushing surface. This leads to an increase in the contact forces and the formation of an extra contact area. Increase of contact forces raises the frictional heat flux and sets up a positive feedback that accelerates the loss of clearance. The increase in the frictional torque is abrupt once the ovalization of the bearing causes the shaft to encroach the bushing, as there is further loss in the operating clearance. The frictional torque increased to exceedingly large values within typically 3 seconds after the first instance of establishment of new areas of contact. The reasons for such an abrupt increase in frictional torque are:

(i) As explained previously, the increase in contact forces increases the frictional heat generated and the increase in frictional heat means that the shaft would expand more increasing the contact forces and establishing more area of contact. This process leads to a positive feedback loop and a chain reaction leading to a rapid failure due to TIS.

(ii) The operating clearance of the bearing just before seizure is reduced to a significantly lower value compared to the steady-state operating clearance. This is due to the thermal expansion of the journal and the bearing into the operating clearance area. The available

clearance just before the extra contact occurs has already reduced to an exceedingly small value. The following plots, Figures 4.4 - 4.6 illustrate the onset and completion of seizure for a journal bearing during start-up. The operating parameters are listed below:

$W$ = 4400 N
$N$ = 250 rpm
$R_s$ = 25.5 x $10^{-3}$ m
$R_b$ = 51.0 x $10^{-3}$ m
$C$ = 0.0125 x $10^{-3}$ m
$L$ = 51.0 x $10^{-3}$ m

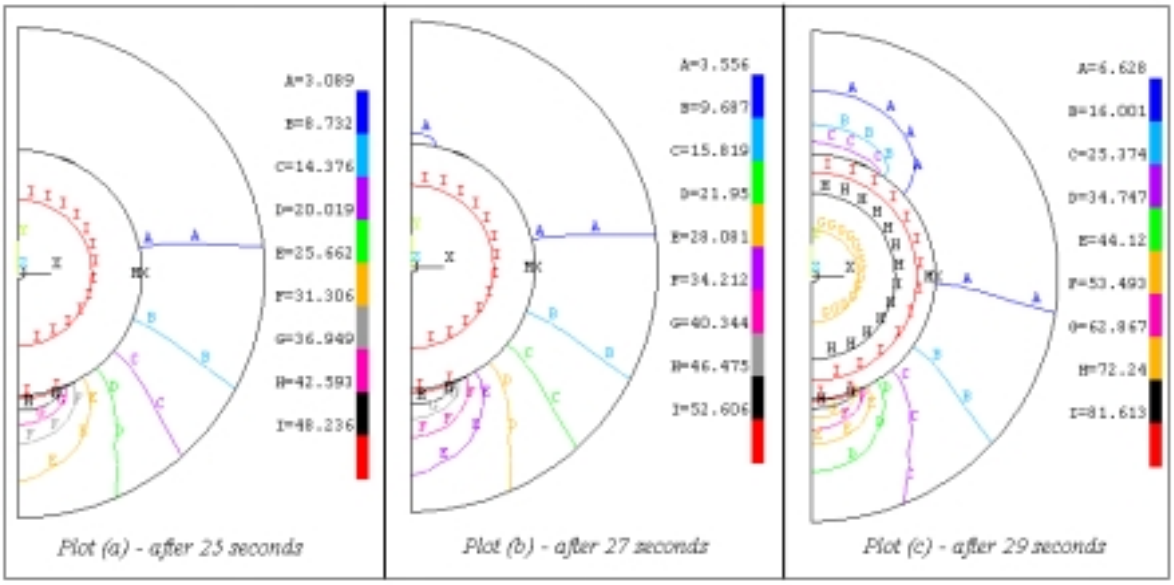


Figure 4.4 – Temperature rise as a function of time in a journal bearing during start up
Plot (a) – Temperature rise, 25 seconds after starting
Plot (b) - Temperature rise, 27 seconds after starting. Note the ovalization and establishment of extra contact, A, at the top of bearing
Plot (c) - Isothermal plot of temperature rise, 29 seconds after starting – Note the formation of extra areas of contact and rapid temperature rise

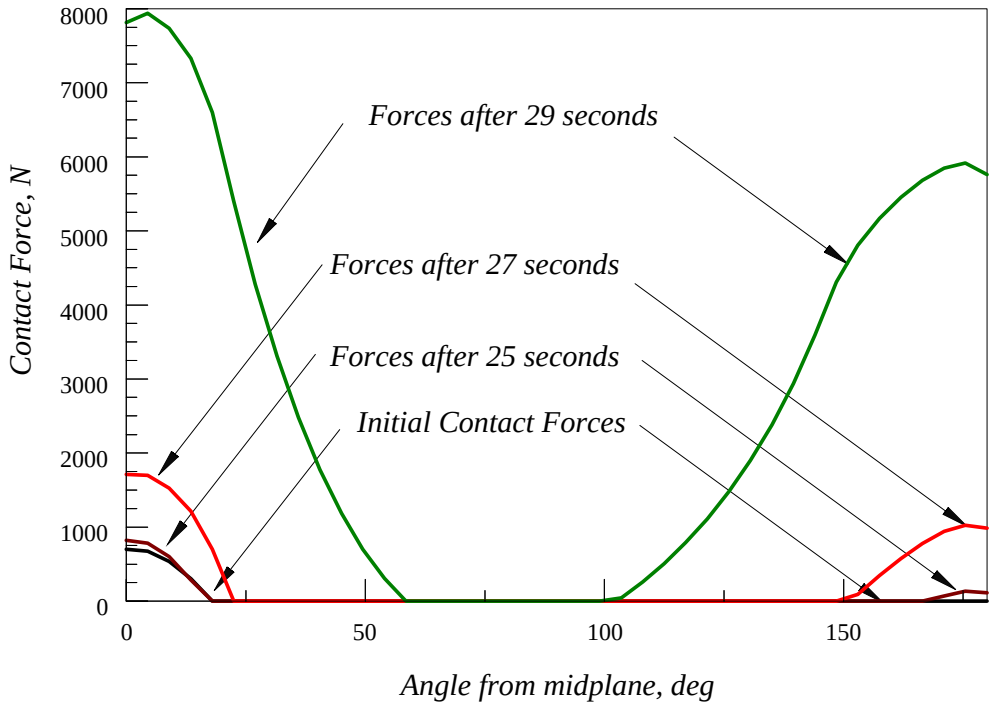


Figure 4.5 - Variation of contact forces with time during start-up

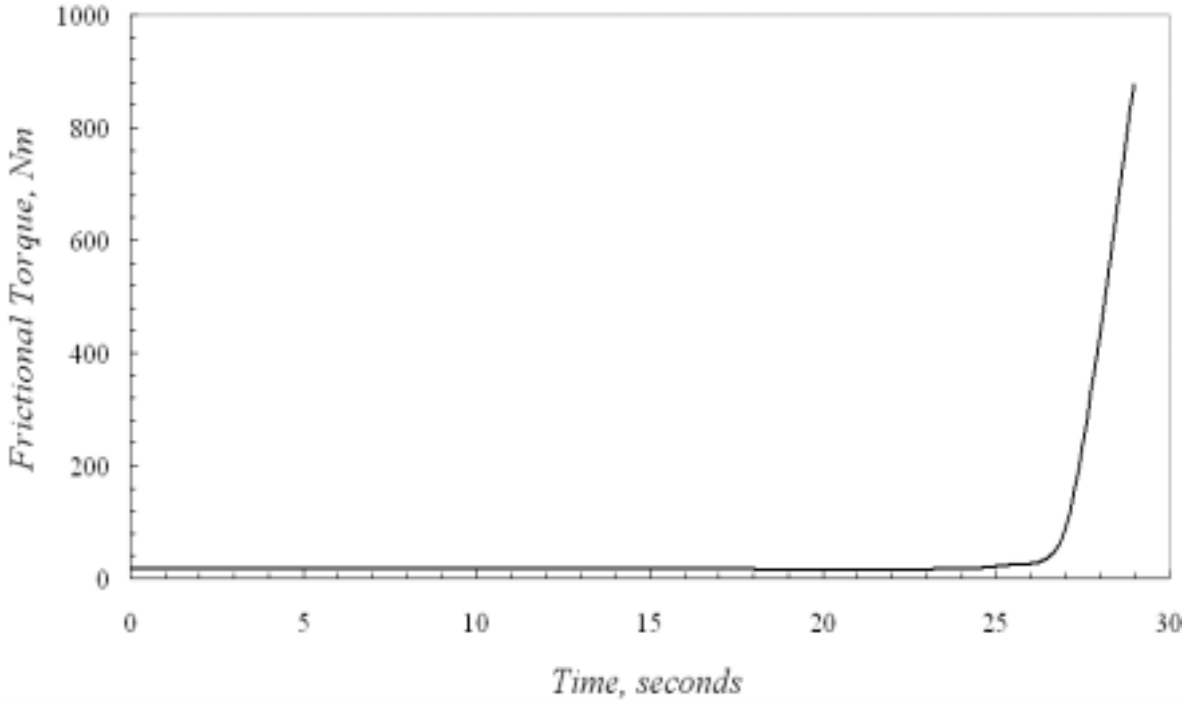


Figure 4.6 - Variation of frictional torque during start-up – Note that the frictional torque increased to 50 times the initial frictional torque to indicate seizure

Figure 4.4 (a) shows temperature rise on the journal bearing pair just before ovalization. Figure 4.4 (b) shows the initiation of extra contact at the top of the bearing. Figure 4.4 (c) shows the temperature increase after 2 seconds after the establishment of extra areas of contact, which illustrates the substantial rise in temperature and contact area. Figures 4.5 and 4.6 show the variation of contact forces and frictional torque over time. It is interesting to note from Figures 4.4-4.6 that, although the frictional torque increased to 50 times the initial torque, the clearance has not reduced to zero clearance at all points proving that the frictional torque is a better seizure criteria than zero-clearance. These simulations reveal that the frictional torque reaches very high values after approximately 3 seconds after ovalization is first experienced. The ovalization is realized in the analysis when additional contact is established at the top of the bearing. Therefore, it will be assumed that the seizure is complete 3 seconds after the first instance of ovalization. Additional simulations with difficult operating conditions also reveal that this condition holds.

**4.3 Model Parameters**

The model used to study the effects of TIS during bearing start-up is given in Table 4.1. The ranges of the operating variables were arrived by taking the operating parameters used by Dufrane and Kannel [7] for experimentation and by Kim and Khonsari [8] and by Hazlett and Khonsari [10] for doing the analytical and finite element modeling as the basis. The parameters used are:

Table 4.1 – Operating parameters for the finite element model and simulations

| | |
|---|---|
| Range of shaft radii, $R_s$ (m) | $10 \times 10^{-3}$ - $37.5 \times 10^{-3}$ |
| Range of bearing lengths, $L$ (m) | $51 \times 10^{-3}$ -$100 \times 10^{-3}$ |
| $\rho C_p$ (N/m$^2$K) | $1.23 \times 10^{6}$ |
| Conductivity, $K$ (W/mK) | 52 |

| | |
|---|---|
| $\alpha$ (m/mK) | $0.3 \times 10^{-5} - 2 \times 10^{-5}$ |
| Young's modulus of shaft, $E_s$ (GPa) | 200 |
| Young's modulus of bush, $E_b$ (GPa) | 110 |
| Poisson's ratio, $\nu_s = \nu_b = \nu$ | 0.3 |
| Range of loads, $W$ (N) | 1000-10000 |
| Range of friction coefficient, $f$ | 0.1 – 0.3 |
| Range of speeds $N$ (rpm) | 150-2000 |
| Range of radial clearances, $C$ (m) | $0.005 \times 10^{-3}$ - $0.0325 \times 10^{-3}$ |
| Convection on all faces, $h$ (W/m$^2$K) | 80 |
| Atmospheric Temperature, $T_\infty$ (°C) | 25 |

**4.4 Generalization**

To derive a relation between the seizure time, $t_s$, and the operating parameters, a statistical procedure followed based on the work done by Hamrock [21].

The seizure time can be written as a function of the various operating parameters.

$$t_s = g\ (N, W, R_s, R_b, C, f, L, \kappa, \alpha).$$

The variation of the seizure time during the system start-up is studied when the operating parameters (variables $N$, $W$, $R_s$, $R_b$, $C$, $f$, $L$ $\kappa$, $\alpha$) are varied. Then a generalized equation is derived depending on the individual relationships of the operating parameters with the seizure time.

The simulations were performed to establish the effects of the operating parameters on the seizure time during the start-up. The speeds are varied from 150 rpm to 2000 rpm. For speeds lower than 150 rpm, the seizure times are large enough such that the lubricant flow would have been established during starting. For speeds higher than 2000 rpm and the operating clearance specified, the seizure time is nearly the same, about 2 seconds. This means that the seizure time is almost asymptotic with respect to speed. All the other parameters were also varied based on a similar rational. The lower limits of the load and the speed were decided if seizure times exceeded 120 seconds. The reasoning behind this cut-off point is that the lubricant supply would have been

established within 2 minutes of starting the system. The shaft radius was varied from 10 mm to 37.5 mm. The upper limit of the shaft radius was limited as increasing the shaft radius above 37.5 mm meant that the bearing thickness was less than 10 mm. The length of the shaft was varied from long bearings (L/D=2) to short bearings (L/D = 0.5). These are the limits that are generally known as the infinitely long and infinitely short approximations [22] (ILA and ISA). The clearances were decided based on typical operating clearances of journal bearings. The friction coefficient was varied from 0.1 to 0.3. These are typical values of friction coefficients for steel on brass sliding [23].

### 4.4.1 Influence of Operating Parameters

Increasing the speed of the shaft means that the heat generated at the interface of the journal and the bearing increase in a direct proportionality. Seizure time decreases with increasing speed of the shaft.

The effect of increase in load is a proportional increase in the frictional heat generated. This means that the seizure time decreases with increasing load. The influence of load on the seizure time is determined by varying the load from 1100 to 10000 N keeping the other factors ($N$, $R_s$, $R_b$, $C$, $f$, $L$, $\kappa$, $\alpha$) constant.

The influence of radial clearance on the seizure time is determined by varying the load from 0.005 to 0.0325 mm keeping the other factors ($N$, $W$, $R_s$, $R_b$, $f$, $L$, $\kappa$, $\alpha$) constant. A decrease in clearance means that the shaft has lesser room to encroach before contacting the bearing and hence the seizure time decreases with decrease in clearance.

Increase in the shaft radius produces two contrasting effects on the seizure time. Increase of shaft radius means that the surface velocity of the bearing increases for the same speed. This means that the frictional heat generated is increased. But an increase in the radius of the shaft also means that the thermal mass of the shaft is increased. So the net

effect of these two modes of heat generated and heat stored decides whether the bearing seizes faster or slower. It can be inferred from Appendix A that the increase in the shaft radius decreases the time for seizure up to a particular shaft radius. Beyond a shaft radius of 25 mm, the effect of the increased thermal mass nullifies the effect of the increase in the surface velocity. The influence of shaft radius on the seizure time is determined by varying the load from 10 to 37.5 mm keeping the other factors ($N$, $W$, $C$, $R_b$, $f$, $L$, $\alpha$) constant.

The influence of the outside radius of the bushing on the seizure time is determined by varying the outside radius from 32.5 to 100 mm keeping the other factors ($N$, $W$, $R_s$, $C$, $f$, $L$, $\alpha$) constant. It was found that varying the outside diameter has negligible effect on the seizure time. Hazlett [10] varied the convective heat transfer coefficient on the outside radius of the shaft and did not find any appreciable effect on the thermoelastic interactions of the bearing. The variation of outside radius may be significant only for very thin bearings. The simulations were carried out for bearings with $R_s/t_h$ = 2.0 (thin bearings) to $R_s/t_h$ = 0.5 (thick bearings) and they seized at around the same time. Therefore for most applications, the effect of outside radius of the bushing on the seizure time can be neglected.

The influence of coefficient of friction on bearing seizure time is similar to the effect of speed. Increasing the coefficient of friction increases the heat generated thus reducing the seizure time. The influence of the coefficient of friction is determined by varying the friction coefficient from 0.1 to 0.3 while keeping the other operating parameters ($N$, $W$, $R_s$, $R_b$, $C$, $L$, $f$, $\alpha$) constant.

The influence of bearing length on the seizure time is determined by varying the length from 50 to 100 mm keeping the other factors ($N$, $W$, $R_s$, $R_b$, $f$, $C$, $\alpha$) constant. The effect of the bearing length is two-fold; (i) The increase in bearing length increases the Hertzian contact width meaning the area of heating on the bushing is more, (ii) The increase in bearing length means that the bearing area, $R_s*\theta*L$ would also increase.

**4.5 Non- Dimensionalization**

In order for the analyses and the corresponding statistical procedure to be relevant to any journal-bearing system irrespective of the units used, use of non-dimensional parameters is preferable. The non-dimensionalization scheme utilizes only two non-dimensional operating parameters, while the analyses were carried out for 6 operating parameters. All the operational variables namely load speed and coefficient of friction were combined to get a single non-dimensional parameter and all the dimensional variables like operating clearance, shaft radius and the bearing length were combined into another non-dimensional parameter as described below.

Non-dimensional seizure time during start-up: $\overline{t_{ss}} = \dfrac{t_{ss}\kappa}{R_s^{\,2}}$

Thermal strain: $\varepsilon = \dfrac{fW\omega\alpha}{k_s}$

Modified aspect ratio: $\lambda = \dfrac{R_{eq}}{L}$ , where $R_{eq} = \dfrac{R_s R_{bi}}{R_{bi} - R_s} = \dfrac{R_s(R_s + C)}{C}$

**4.5.1 Statistical Treatment of Non-dimensional Operating Parameters**

A power series equation is used to find the relation between non-dimensional thermal strain and non-dimensional seizure time. The equation derived fits the data with a goodness value of 98.64% as shown in Figure 4.7.

The relation between the non-dimensional seizure time and thermal strain is given by the following equation (4.5)

$$\overline{t_{ss}} = 0.0031\varepsilon^{-1.2478}$$

$$\Rightarrow \quad \overline{t_{ss}} \propto \varepsilon^{-1.2478} \tag{4.5}$$

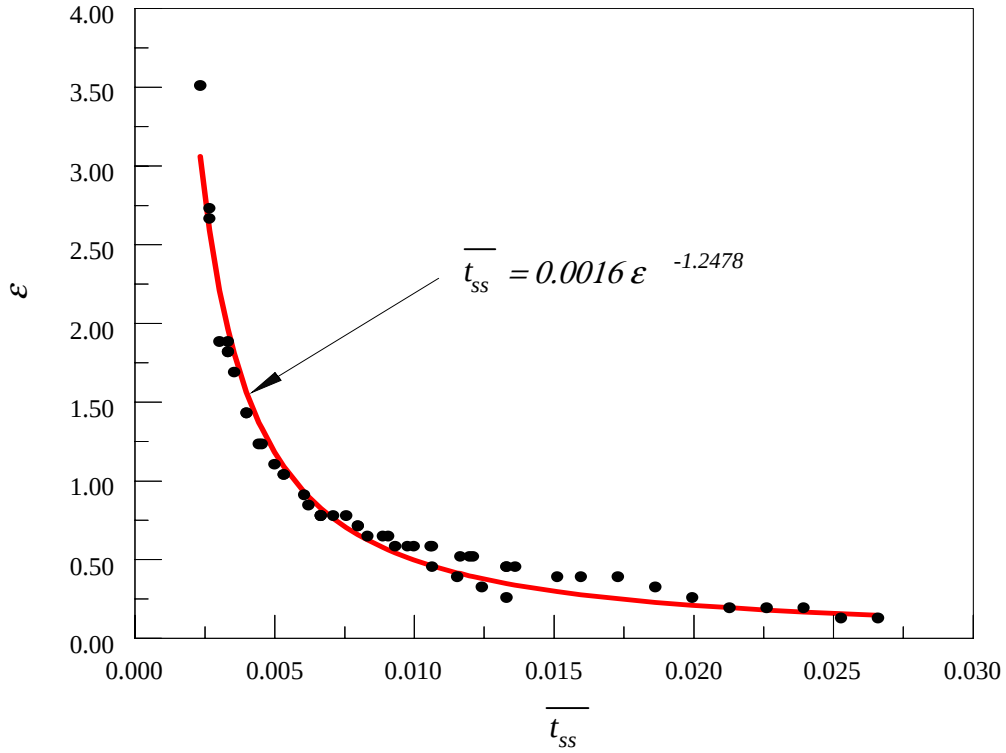


Figure 4.8 – Variation of non-dimensional seizure time with thermal strain

Let us define parameter Γ as

$$\Gamma = \frac{\overline{t_{ss}}}{\varepsilon^{-1.2478}} \tag{4.6}$$

The relationship between the parameter Γ and the modified aspect ratio was also derived using power series expressions. The variation of Γ with modified aspect ratio depends on a particular range of $R_s/C$ values. Two ranges of $R_s/C$ values were considered for the simulations performed and the equation derived fits the data with a goodness value of 97.9% and is given by Equation 4.7.

$$\Gamma = 90.494\ \varepsilon^{-1.6494} \qquad \text{For } 500 > R_s/C > 1000 \qquad (4.7)$$

$$= 1.825\ \varepsilon^{-1.02718} \qquad \text{For } 1000 > R_s/C > 5100$$

$$\Rightarrow \quad \overline{t_{ss}} = 90.494\ \varepsilon^{-1.2478}\lambda^{-1.6494} \qquad \text{For } 500 > R_s/C > 1000 \qquad (4.8)$$

$$\overline{t_{ss}} = 1.825\ \varepsilon^{-1.2478}\lambda^{-1.02718} \qquad \text{For } 1000 > R_s/C > 5100$$

**4.6 Verification and Analysis**

The above empirical relationship (4.8) is verified for its validity using some of the results published by Hazlett and Khonsari [9,10], Wang, Conry and Cusano [11,12] and Bishop and Ettles [6].

The first four cases correspond to the simulations reported by Hazlett and Khonsari [9,10] for journal bearings, the fifth and sixth cases were reported by Hao Wang [11,12] for an analysis dealing with axle burn-off in railroad roller bearings and cases 7 through 17 were reported by Bishop and Ettles in their study of TIS in journal bearings. As can be seen from Table 4.2, the empirical results are in agreement with published results.

In the axle burn-off studied by Hao Wang [12], the nominal operating clearances ranged from 0.05 mm to 5 mm and the axle bearing was lubricated by grease due to very heavy loading and the material properties were reported as functions of temperatures. The material properties used in Table 4.2 for the fifth and sixth cases were averaged values. Wang et al.[6] reported a number of additional analyses with axle bearings. However, a number of the clearances were outside the range of simulations presented in this study and were not considered. Therefore only the 0.05 mm simulations reported was considered for verification. Applying the empirical relation for the other reported clearances would lead to erroneous predictions.

Table 4.2 - Comparison of Empirical results with published results

| No. | Speed rpm | Load N | Clearance m | Shaft Radius, m | Bearing Length m | Thermal conductivity W/mK | Thermal diffusivity $m^2/s$ | Coefficient of friction | Coefficient of thermal expansion, m/mK | Seizure time published, sec | Seizure time calculated, sec |
|---|---|---|---|---|---|---|---|---|---|---|---|
| 1 | 250 | 4400 | $1.25x10^{-5}$ | 0.0255 | 0.051 | 52 | $4.23x10^{-5}$ | 0.15 | $1x10^{-5}$ | 28 | 28 |
| 2 | 1800 | 4400 | $1.25x10^{-5}$ | 0.0255 | 0.051 | 52 | $4.23x10^{-5}$ | 0.15 | $1x10^{-5}$ | 2 | 2.4 |
| 3 | 250 | 4400 | $1.25x10^{-5}$ | 0.0255 | 0.03825 | 52 | $4.23x10^{-5}$ | 0.15 | $1x10^{-5}$ | 21 | 21 |
| 4 | 250 | 4400 | $1.25x10^{-5}$ | 0.0255 | 0.0255 | 52 | $4.23x10^{-5}$ | 0.15 | $1x10^{-5}$ | 16 | 14 |
| 5 | 560 | 160000 | $5x10^{-5}$ | 0.0781 | 0.1562 | 30 | $5.47x10^{-6}$ | 0.3 | $1.3x10^{-5}$ | 3 | 1.3 |
| 6 | 560 | 160000 | $50x10^{-5}$ | 0.0781 | 0.1562 | 30 | $5.47x10^{-6}$ | 0.3 | $1.3x10^{-5}$ | 60 | 59 |
| 7 | 1000 | $1 \times 10^6$ | $0.5x10^{-5}$ | 0.5 | 1 | 52 | $1.44x10^{-5}$ | 0.005 | $1.1x10^{-5}$ | 7 | 7.3 |
| 8 | 1000 | $1 \times 10^6$ | $2.5x10^{-5}$ | 0.5 | 1 | 52 | $1.44x10^{-5}$ | 0.005 | $1.1x10^{-5}$ | 42 | 38 |
| 9 | 1000 | $1 \times 10^6$ | $5x10^{-5}$ | 0.5 | 1 | 52 | $1.44x10^{-5}$ | 0.005 | $1.1x10^{-5}$ | 117 | 78 |
| 10 | 1000 | $0.2 \times 10^6$ | $5x10^{-5}$ | 0.5 | 1 | 52 | $1.44x10^{-5}$ | 0.005 | $1.1x10^{-5}$ | 650 | 583 |
| 11 | 1000 | $0.3 \times 10^6$ | $5x10^{-5}$ | 0.5 | 1 | 52 | $1.44x10^{-5}$ | 0.005 | $1.1x10^{-5}$ | 400 | 352 |
| 12 | 1000 | $0.4 \times 10^6$ | $5x10^{-5}$ | 0.5 | 1 | 52 | $1.44x10^{-5}$ | 0.005 | $1.1x10^{-5}$ | 290 | 246 |
| 13 | 1000 | $0.5 \times 10^6$ | $5x10^{-5}$ | 0.5 | 1 | 52 | $1.44x10^{-5}$ | 0.005 | $1.1x10^{-5}$ | 240 | 186 |
| 14 | 1000 | $5 \times 10^6$ | $5x10^{-5}$ | 0.5 | 1 | 52 | $1.44x10^{-5}$ | 0.005 | $1.1x10^{-5}$ | 35 | 11 |
| 15 | 300 | $1 \times 10^6$ | $5x10^{-5}$ | 0.5 | 1 | 52 | $1.44x10^{-5}$ | 0.005 | $1.1x10^{-5}$ | 510 | 351 |
| 16 | 500 | $1 \times 10^6$ | $5x10^{-5}$ | 0.5 | 1 | 52 | $1.44x10^{-5}$ | 0.005 | $1.1x10^{-5}$ | 270 | 186 |
| 17 | 2000 | $1 \times 10^6$ | $5x10^{-5}$ | 0.5 | 1 | 52 | $1.44x10^{-5}$ | 0.005 | $1.1x10^{-5}$ | 50 | 33 |

Bishop and Ettles [6] studied TIS in journal bearings with non-metallic liners using analytical 1-D and a 2-D analysis. Results from the 2-D analysis of TIS in lubricated journal bearings were considered for verification in Table 2. Note that although the simulations done in the present study did not consider fully lubricated cases, the results derived in Equation (4.8) still holds good. The results in Bishop and Ettles' paper were reported till the temperature reached 320° above ambient temperatures that were considered as the burn-off temperature of the linings. The results reported in Table 4.2 were taken when there is complete loss in clearance that was before the limiting temperature was reached.

To gain further insight into the TIS behavior, we plot the change in the operating clearance as a function of time based in Dufrane and Kannel's equation (4.1) and the empirical Equation (4.8) derived in the present study. The result is shown in Figure 4.9 for two heat partitioning factors ($n$ = 0.5 and 1).

ANSYS 5.7 calculates the heat-partitioning factor based on the thermal mass and material properties at the contact area such that there is continuity of temperature and flux at the contact interface. A heat partitioning of 1 is unreasonable as it means that all the frictional heat generated would be transmitted into the shaft. The analyses done by Dufrane and Kannel [7] did not consider the expansion of the bushing and the thermal expansion of the shaft was only considered. Also, the bushing was rigidly constrained. As the present study has considered the bushing constraint the outward expansion of the bushing, the seizure times were larger than the values obtained using Equation (4.1) used by Dufrane and Kannel. From Figure 7, it can be seen that the present model compares close to Dufrane and Kannel's model when a heat-partitioning factor of 0.5 is used in

Equation (1). The seizure time formula developed in this study predicts the loss of clearance with time is not a linear process. Whereas Equation (4.1) implies that TIS occurs regardless of the size of the clearance, the predicted results here reveal that this is not true for large clearances. This physically realistic prediction was first discussed by Khonsari and Kim [24].

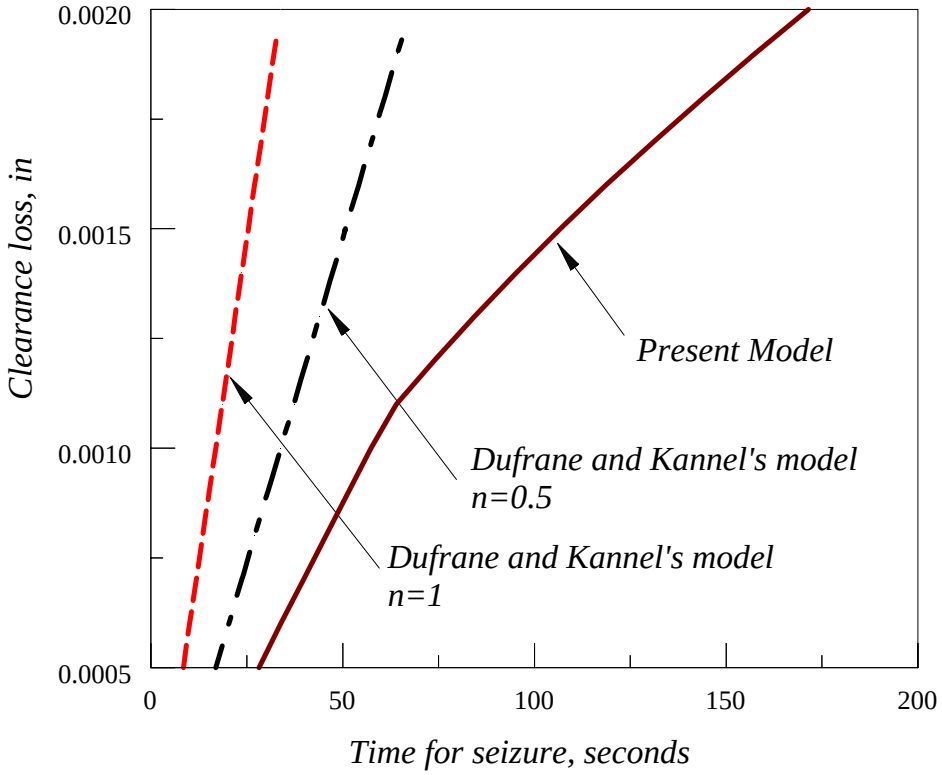


Figure 4.9 – Comparison of seizure time with Dufrane and Kannel's model and the present model. Note: n = heat partition factor

There are some limitations that restrict the use of these relations depending on the operating conditions.

1. It is recommended to use the empirical relations for operating conditions close to the conditions used in the simulations. This is especially true for the operating clearance.

2. The boundary condition for the fixation of the bearing varies with different applications. The boundary condition used in this analysis allows some flexibility for the bearing to expand outwards. If the bearing were fully constrained, the seizure times would be appreciably reduced.

# CHAPTER 5. TIS OF JOURNAL BEARINGS TRIGGERED BY A TRANSIENT FLOW DISTURBANCE

The thermoelastic interaction of journal bearing pair in the event of a disturbance in lubricant flow is a largely neglected area of study. There are a number of situations whereby a journal bearing system while running steady may suddenly experience a disturbance in its operating conditions. In this part, we focus our attention to the situation whereby a system undergoes a transient flow disturbance. A "lubricant supply perturbation" in an otherwise steady-state operation may be caused by a brief interruption of lubricant supply due to a clogged filter or air locking, for instance. Transient operating conditions are also predominant in aircraft during the periods of taking-off, landing and maneuvering [14].

When the lubrication perturbation occurs for a short period of time, the lubrication regime can shift from hydrodynamic into the mixed and boundary lubrication regime. This transition of the bearing operating conditions from the thick-film to the boundary lubrication regime can significantly affect the operating coefficient of friction and the convective heat transfer coefficient within the clearance. Ideally once the lubricant supply is resumed, the bearing reverts back to the thick-film regime, otherwise TIS becomes imminent. Evaluation of the thermomechanical response following the resumption of lubricant supply is necessary to understand if the system can survive the interruption of lubricant flow.

In this chapter, flow interruption is modeled as a transition between various lubrication regimes. This transition is assumed to take place linearly with time. The methodology behind the application of the lubricant perturbation can be graphically represented by Figure 5.1 and 5.2. Lubricant flow disturbance is assumed to occur over a

period of 150 seconds from the onset of the disturbance to full resumption of steady operation. This period consists of an initial rise in the coefficient of friction and concomitant reduction of convective heat transfer coefficient over a period of 70 seconds, during which there is a gradual transition from full-film to boundary lubrication. Then, a duration of 10 seconds in the boundary lubrication followed by a 70 seconds transition to full-film lubrication is assumed. The coefficient of friction for the fully lubricated bearing is typically in the order of 0.005. During the transition regime, the coefficient of friction is ramped linearly with time to 0.15, which represents lubricated metal-to-metal sliding.

A convective heat transfer coefficient of 200 $W/m^2K$ is assumed for thick-film lubrication. During the transition period of 70 seconds, the convective heat transfer coefficient is ramped linearly till the HT coefficient reaches 80 $W/m^2K$ as shown in Figure 5.2. The nominal convective coefficient for air at the speeds involved is around 80 $W/m^2K$ [9,10]. A change in the steady-state thick-film heat transfer coefficient was found to have minimal effect on the bearing seizure time as the seizure occurs primarily due to the flow disturbance and not due to the steady-state temperature rise.

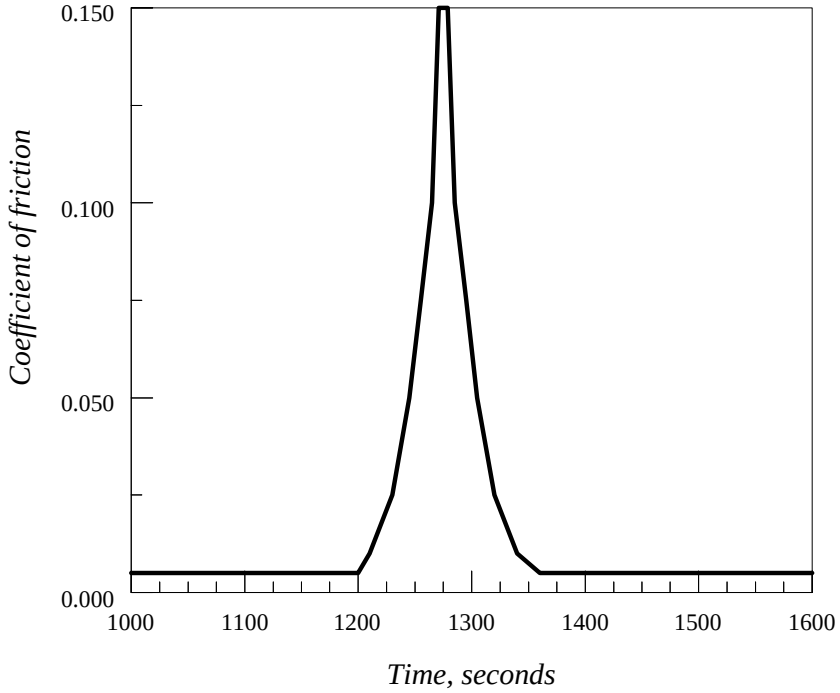


Figure 5.1 – Variation of friction coefficient during lubricant perturbation

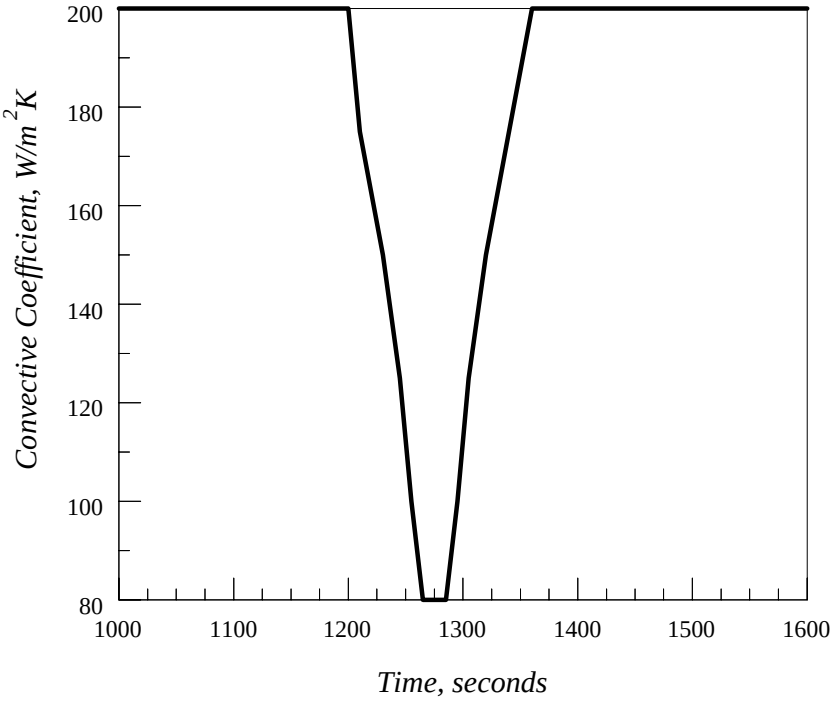


Figure 5.2 – Variation of convective HT coefficient during lubricant perturbation

## 5.1 Finite Element Analysis Modeling and Seizure Criteria

The procedure and modeling approach is similar to Section 4, where TIS during bearing start-up was studied with a few minor differences. The thermal analysis is performed at thick-film hydrodynamic conditions until steady state is achieved and then the transient flow disturbance is applied in the transient. The finite element procedure overview is given below

1. A 2-D static contact analysis was performed to determine the contact forces and the contact angle.
2. A transient heat transfer analysis was done to determine the time required for the journal bearing to attain the steady-state conditions. The perturbation conditions (increase in coefficient of friction and decrease in the convective heat transfer coefficient) were applied after the time required for the journal-bearing pair to reach steady state. The methodology of the application of the lubricant perturbation is done as per the procedure described in Section 5.0 (Figures 5.1 and 5.2).
3. A transient thermoelastic analysis was performed to study the interactions of the journal-bearing pair under the influence of perturbation. The variation of radial clearance, contact forces and ovalization of the bearing were studied in this analysis.

The bearing seizure is assumed to be complete when the frictional torque greatly exceeds the driving torque. This is similar to the methodology explained in Section 4.1.3

## 5.2 Results and Discussion

The failure of journal bearings undergoing a transient disturbance in flow is primarily due to the seizure of the shaft in the bearing due to thermal expansion of the shaft and the bearing and concomitant reduction in clearance. This process is similar to the TIS of bearings during start up. The time to seize differs from the TIS of bearings during start up. This is due to the fact that the increase in the coefficient of friction and the reduction of convective heat transfer is gradual as the bearing moves from a thick-film regime to boundary lubrication over a period of time. The thermomechanical process of seizure is explained for a journal bearing with the same operating conditions as discussed in Section 4 is discussed in this section.

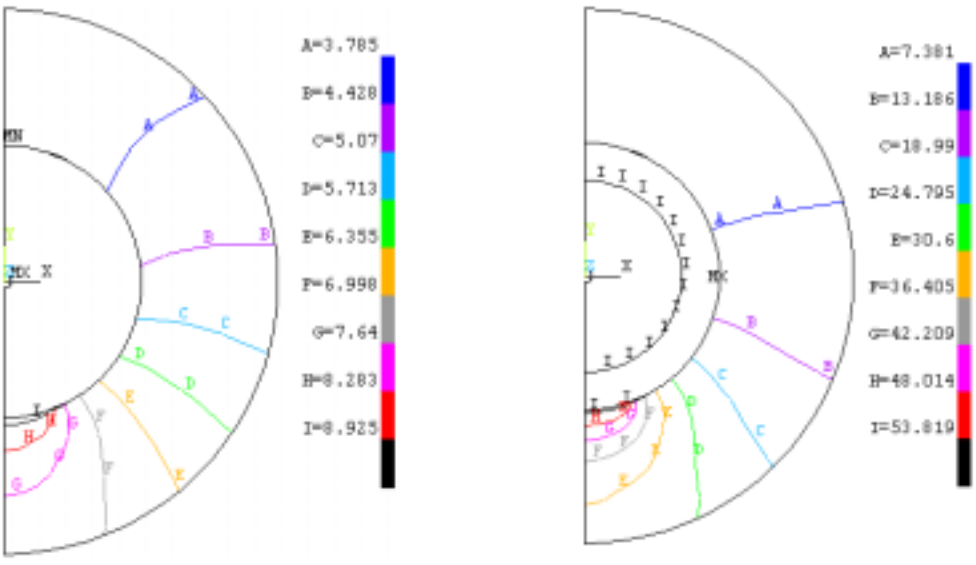


*Plot (a) – Steady state temperature rise*

*Plot (b) – after 62 seconds*

Figure 5.3a, b – Plots of temperature rise during a transient flow disturbance

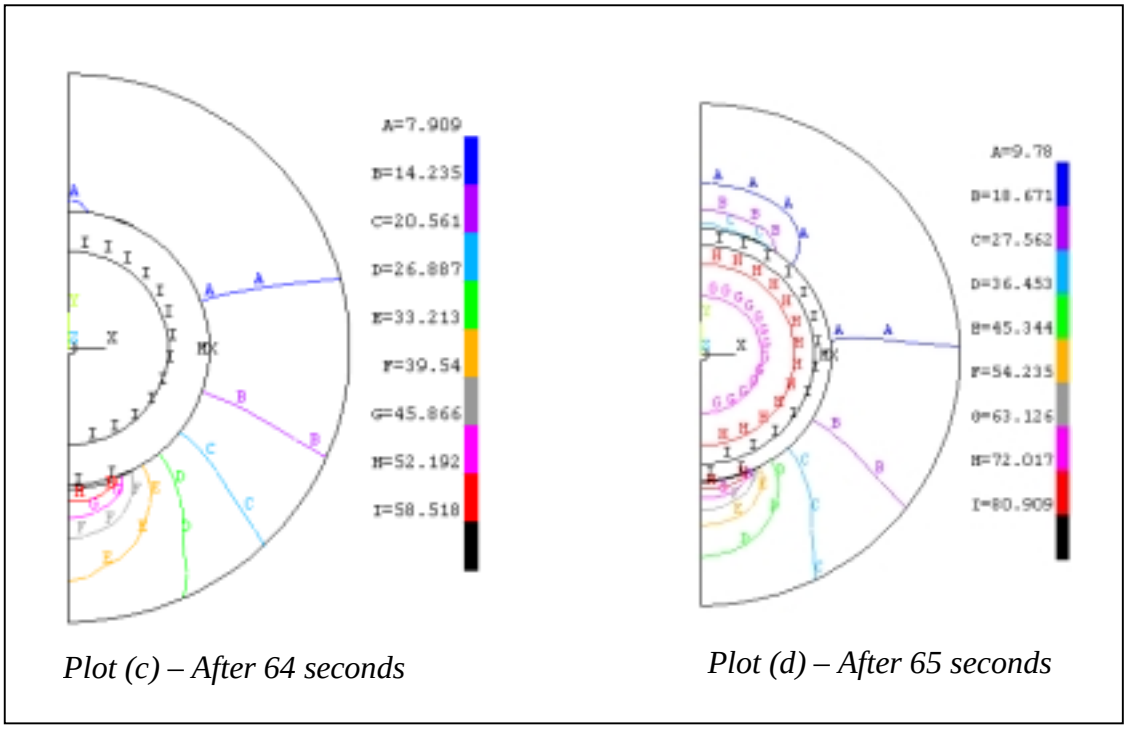


*Plot (c) – After 64 seconds*

*Plot (d) – After 65 seconds*

Figure 5.3c,d – Plots of temperature rise during a transient flow disturbance

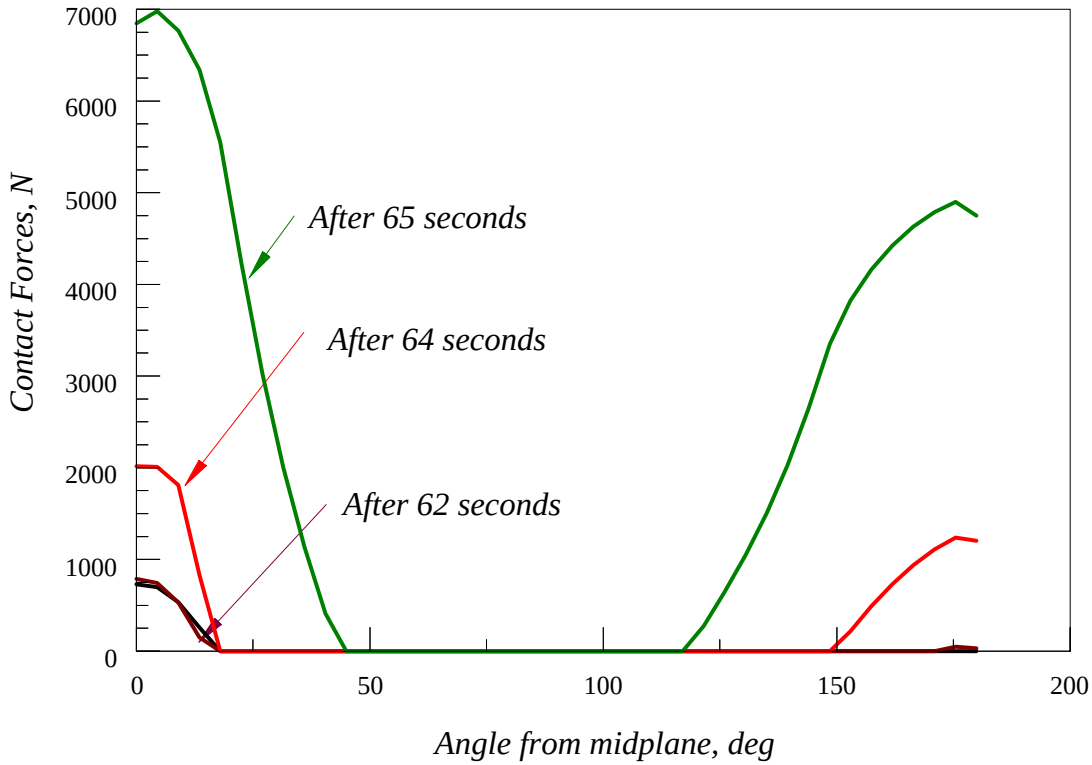


Figure 5.4 - Variation of contact force after the onset of ovalization due to flow disturbance

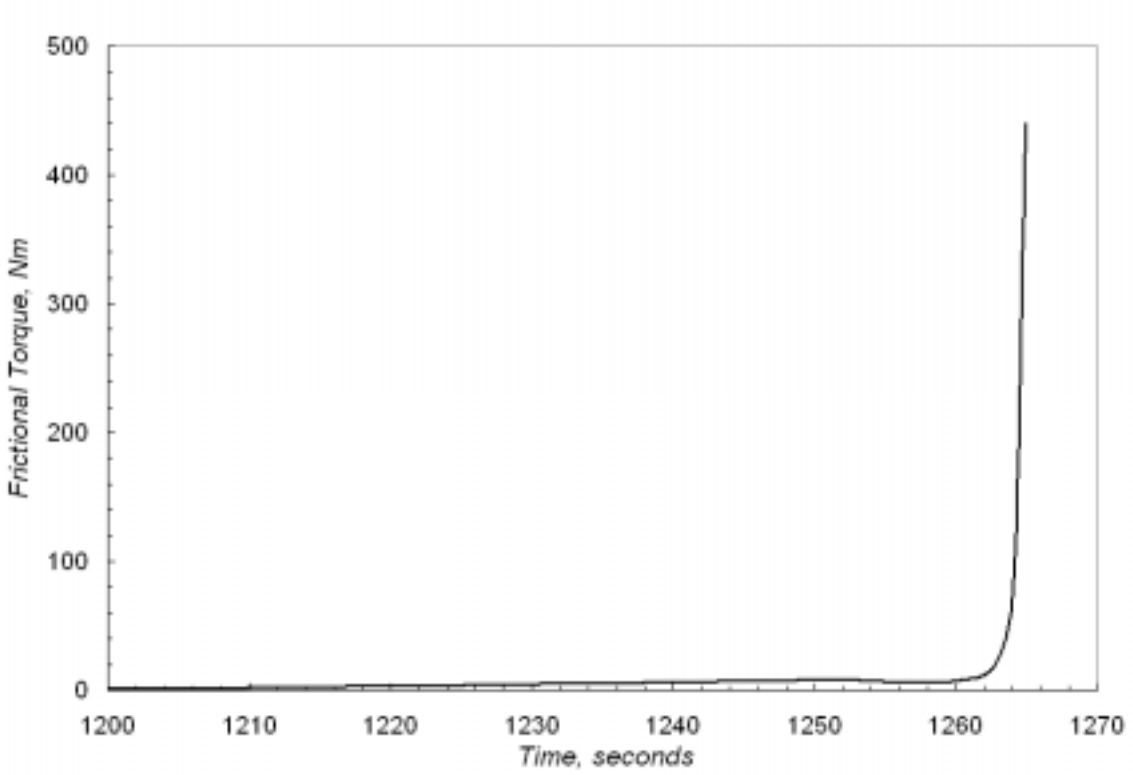


Figure 5.5 – Variation of frictional torque when a transient flow disturbance occurred

Comparing Figures 5.3 through 5.5 with Figures 4.4 through 4.6, it can be seen that the process of TIS follows a similar procedure, the only difference being the time taken to seize. It is an interesting fact that the ovalization of the bearing and the establishment of the extra areas of contact contributed to the rapid seizure of the bearing in the case of flow interruption also.

**5.3 Model Parameters**

The model parameters are similar to Table 4.1, except that the operating parameters are of a wider range than that of the start up analysis.

Table 5.1. Operating parameters for simulating TIS in a journal bearing undergoing a transient flow disturbance

| | |
|---|---|
| Shaft Radius, $R_s$ (m) | $10 \times 10^{-3}$ -$37.5 \times 10^{-3}$ |
| Length of Bush, $L$ (m) | $51 \times 10^{-3}$ -$100 \times 10^{-3}$ |
| $\rho C_p$ (N/mm$^2$K) | 1.23 |

| | |
|---|---|
| Conductivity, $K$ (W/mK) | 52 |
| $\alpha$ (mm/mmK) | 1e-5 |
| Young's Modulus of Shaft, $E_s$ (GPa) | 200 |
| Young's Modulus of Bush, $E_b$ (GPa) | 110 |
| Poisson's Ratio, $\nu_s = \nu_b$ | 0.3 |
| Load, $W$ (N) | 2200-12000 |
| Friction Coefficient, $f$ | 0.15 |
| Speed, $N$ (rpm) | 500-3000 |
| Radial Clearance, $C$ (m) | $0.0125 \times 10^{-3}$ |
| Convection on outer face, $h$ (W/m$^2$K) | 80 |
| Atmospheric Temperature, $T_\infty$ (°C) | 25 |
| Transition time, $t_{ref}$ (sec) | 20-100 |

### 5.4 Non-Dimensionalization and Generalization

Similar to Section 4.4, a statistical analysis was performed and an empirical relationship was derived for arriving at the seizure time when a journal bearing undergoes an interruption in lubricant supply. As the analysis procedure is different from the thermoelastic analysis done for predicting seizure time, a different non-dimensionalization technique was followed. The non-dimensional parameters used in the analysis are defined below.

Non-dimensional seizure time, $\overline{t_s} = \dfrac{t_s}{t_{ref}}$

Non-dimensional seizure time during flow disturbance: $\overline{t_{sp}} = \dfrac{t_{sp}}{t_{ref}}$

Thermal strain: $\varepsilon = \dfrac{fW\omega\alpha}{k_s}$

Modified aspect ratio: $\lambda = \dfrac{R_{eq}}{L}$, where $R_{eq} = \dfrac{R_s R_{bi}}{R_{bi} - R_s} = \dfrac{R_s(R_s + C)}{C}$

Using the results of 50 sets of results, the relationship between the non-dimensional time for seizure and the non-dimensional operating parameters is given by the following equation (5.1).

$$\overline{t_{sp}} = \left(\varepsilon^{0.5489}\left(0.0065\lambda + 9.314\right)\right)^{-1} \qquad (5.1)$$

**5.5 Analysis of Results**

The empirical relation (5.1) provides a useful empirical relation about the seizure time to be expected when a bearing undergoes a disturbance in lubricant supply. The physical meaning of the seizure time and restrictions of the empirical relation (5.1) are explained next.

1. If the empirical relationship predicts a seizure time of, say 48 seconds, it means that the bearing failed in the transition period before boundary conditions are achieved. If a bearing seizes between 71 and 80 seconds it means that the seizure is during the boundary lubrication period. Similarly if seizure time is greater than 80 seconds, it means that the seizure has taken place after the lubrication is restored.
2. For bearings that seize within 70 seconds, i.e. before the mixed/boundary lubrication phase occurs, it means that those bearings cannot sustain even a lubricant cut-off for a few seconds. Most of the cases considered in this analysis falls within this category.
3. The empirical relationship does not apply to bearings that may be susceptible to seizure in hydrodynamic regime. Some heavily loaded bearings that operate at high speeds or with low clearances may seize in fully lubricated conditions. When the empirical formula (5.1) is applied for these conditions, they give a finite value

of seizure time when the bearing had already seized even with no perturbation. Typically, seizure times of 20 seconds or below fall under this category. If the empirical relationship yields a result of 20 seconds or lower, it means that the bearing has already seized or it would seize even for a slight change in the operating conditions. The TIS failure of lubricated journal bearings has been studied by Pascovici et.al. [15] where a "no-seizure" condition was arrived based on the bearing operating parameters. Jang et.al. [16] performed an extensive study of TIS in thick film journal bearings. The thermoelastic behavior was theoretically formulated and experimentally verified.

4. The material properties used in the simulations pertain to mild steel shaft and bronze bearing. So the above empirical relations can be used only for material combinations that are close to the material properties of the materials that were used in the simulations. Most of the bearing materials typically have a bronze base and shaft made of steel. That was the reason behind choosing this material pair.
5. The Finite Element Analysis neglected the heat transfer in the axial direction. Only a 2D analysis was performed.
6. The analysis is valid in the transition time ranges of 20 to 80 seconds. The transition time is the time taken for the bearing to go from fully lubricated mode to boundary lubrication mode.
7. The boundary conditions for the fixation of the bearing vary with different applications. The boundary conditions used in this analysis allow some flexibility

for the bearing to expand outwards. If the bearing were fully constrained, the seizure times would be appreciably reduced.

### 5.6 Verification

A verification is performed for some operating conditions and the validity of the empirical relation is checked against the simulated results obtained from ANSYS finite element simulations for the following operating conditions.

$$W = 8800 \text{ N}$$
$$N = 500 – 2400 \text{ rpm}$$
$$C = 0.0255 \text{ x } 10^{-3} \text{ m}$$
$$R_s = 0.0255 \text{ m}$$
$$R_b = 0.051 \text{ m}$$
$$L = 0.051 \text{ m}$$

For the above operating conditions, the results of the empirical relation are compared to the results of the simulations performed using ANSYS 5.7. The results are tabulated in Table 5.2. The % error was computed and the max error was found to be 7.5%. The comparison is repeated for other simulations also. It was found that the empirical relation provides a realistic and conservative estimate for seizure time for most of the cases.

Table 5.2 – Comparison of simulated seizure time and empirical seizure time

| Speed | Empirical Seizure Time | Simulated Seizure time | %error |
|---|---|---|---|
| 250 | 99 | 100 | -1.01 |
| 500 | 67 | 68 | -1.49 |
| 750 | 53 | 58 | -1.89 |
| 1000 | 45 | 50 | -4.44 |
| 1200 | 40 | 46 | -5.00 |
| 1400 | 37 | 44 | -5.41 |
| 1600 | 34 | 38 | -5.88 |
| 1800 | 32 | 34 | -3.13 |
| 2000 | 30 | 30 | -6.67 |
| 2200 | 28 | 30 | -7.14 |
| 2400 | 27 | 26 | -7.41 |

An interesting observation can be made from Table 5.2 for the operating speed of 250 rpm. The seizure time predicted by the empirical formula and from the simulations is about 100 seconds. This means that the bearing seized even after the resumption of lubricant supply.

# CHAPTER 6. THERMOMECHANICAL ANALYSIS OF A HEAVILY LOADED OSCILLATING PIN-BUSHING PAIR

## 6.1 Introduction and Problem Definition

Heavy-duty earth-moving machinery use linkages that are supported on a pin and bushing pair. They are subject to very heavy loads generally operating at low speeds. Typically in the pin-bushing pair, the pin is stationary while the bushing oscillates at low frequencies. These pin-bushing pairs are typically made of mild steel and surface treated with a protective coating. Depending on the application, the pin-bushing pair maybe packed with grease during assembly. Industry is now using automatic grease feeders or recommends feeding grease periodically. There is no provision for a continuous supply of lubrication in the system and the packed grease is the only source for lubrication. After some time of operation in field, the pin-bushing pair exhausts the supply of grease packed in the assembly by normal operational leak as well as wear and tear. The absence of proper lubrication leads to the wear of the anti-friction liner on the surfaces of the pin-bushing pair. Further operation causes intimate metal-to-metal contact between the pin and the bushing that leads to high heat generation in the contact region. The absence of proper lubrication, very high loads and improper cooling leads to failure of the bearing either by galling or by thermally induced seizure (TIS). A typical schematic of the pin-bushing oscillating pair used in the undercarriage of heavy-duty earth-moving equipment is shown in Figure 6.1.

Galling is defined as the mode of failure when there is plastic deformation and localized welding of relative moving parts and subsequent wear of the welded parts due to the shear loads. Galling can occur due to very high stresses and/or due to very high rise in temperatures. The combination of heavy loads and high temperatures in the oscillating

pin-bushing assembly in earth-moving machinery makes it vulnerable to galling. Thermally Induced Seizure (TIS), on the other hand, is the mechanism of failure if there is a complete loss in operating clearance in the pin-bushing assembly as the pin encroaches into the bushing. The underlying phenomenon is similar to that described in Chapters 4 and 5, except that in the oscillating pin-bushing assemblies, the temperatures involved and the time to failure are generally higher. Once failure starts the surface temperature at the pin-bushing interface shoots up to very high values introducing possible galling or TIS, depending on the operating conditions.

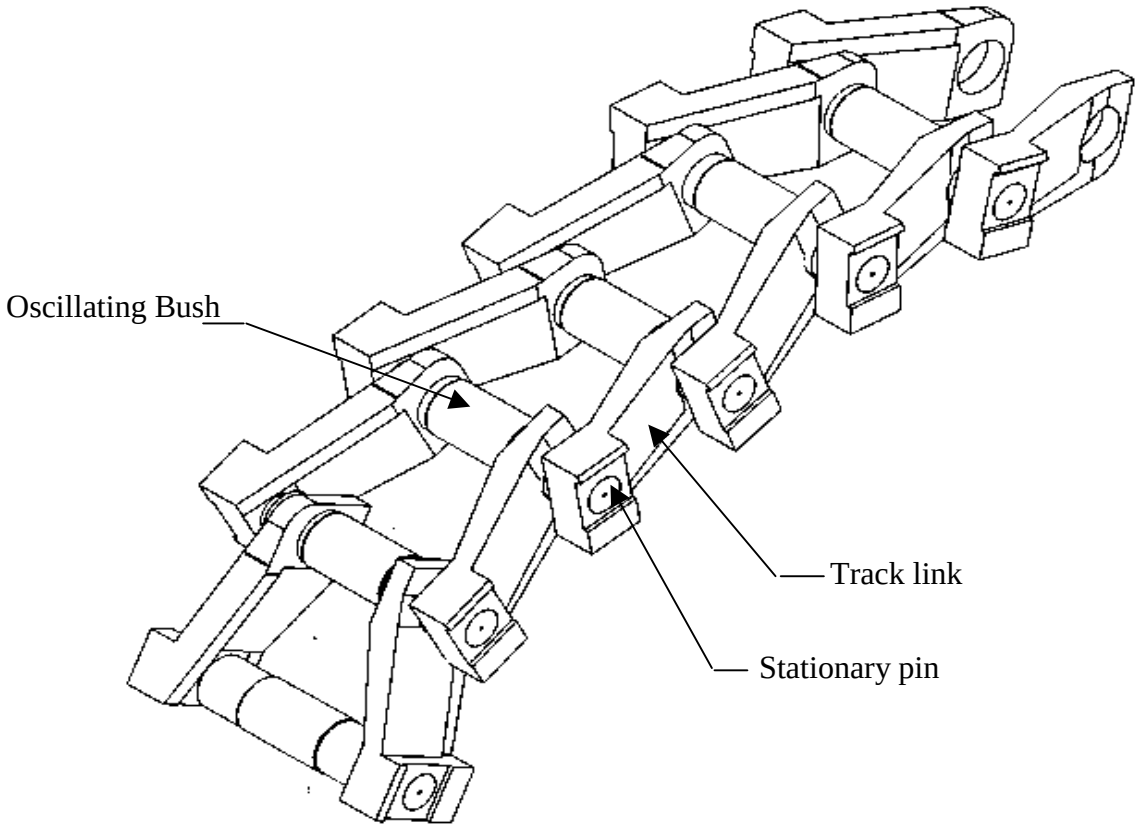


Figure 6.1 – Track Retention Assembly with the oscillating pin and bushing

## 6.2 Problem Description and Solution Methodology

The objective of the work done in this chapter is to study the thermomechanical interactions of an oscillating pin-bushing pair undergoing oscillating loading conditions. The finite element method is used to perform thermal and thermomechanical simulations to determine the performance of the oscillating pin-bushing pair at various operating conditions. The objective of this research is to develop an analysis for predicting failure of pin-bushing under oscillating loads.

The problem is solved in a 3-step routine described briefly below and in detail in sections 6.4 to 6.6.

(i) Theoretical Hertzian contact analysis

(ii) Transient finite element thermal analysis using ANSYS 5.7

(iii) Transient finite element thermomechanical using ANSYS 5.7

## 6.3 Theoretical Hertzian Contact Analysis

A theoretical analysis is performed as first steps to determine the contact forces and ascertain the contact patch using Hertzian theory of elastic contact[21]. The contact area and the contact pressure are calculated from the Hertzian theory of elastic contact. For a line contact, the Hertzian half-contact width is given by Equation (6.1) [21] as,

$$b = 1.598\sqrt{\frac{wR}{LE}} \qquad (6.1)$$

where

$b$ = semi-contact width, m

$w$ = Load acting on the pin, N

$R$ = Equivalent Radius of contact, m

$L$ = Length of contact in the normal direction, m

$E$ = Equivalent Elasticity modulus, $N/m^2$

The contact region is measured using the equivalent elastic modulus and equivalent radius of contact. For a Hertzian elastic contact, the equivalent radius and the equivalent modulus of elasticity are given by Equations (6.2) and (6.3)

Equivalent radius: $$R = \frac{R_1 R_2}{R_1 \pm R_2} \tag{6.2}$$

Equivalent Young's modulus: $$E = 2\left[\frac{1-\nu_1^{\,2}}{E_1} + \frac{1-\nu_2^{\,2}}{E_2}\right]^{-1} \tag{6.3}$$

where the subscripts *1* and *2* refers to the pin and bushing respectively and the denominator has + for convex contact and – for concave contacts. As a pin and bushing contact is concave, we use the difference of the radii of the pin and bushing as our denominator.

**6.4 Thermal Analysis**

Frictional heat is generated at the interface between the pin and the oscillating bushing when the two surfaces slide against each other. The heat generated is a function of the contact forces, coefficient of friction and the sliding velocity. The heat generated is distributed as per a partition factor between the pin and the bushing. The partition of heat is dependent on the material properties, thermal mass and the relative velocity of the pin and the bushing. The finite element analysis program like ANSYS or FlexPDE [25] can calculate the partition of heat flux automatically taking into account the thermal mass and material properties of the contacting bodies. The objective of the transient thermal analysis is to obtain the time-dependent temperature contours of the pin-bushing under the application of the oscillating frictional heat flux. The results of the transient thermal analysis are used in doing the thermomechanical analysis to determine the pin-bushing interactions.

### 6.4.1 Element Types

The pin and bushing are modeled in ANSYS 5.7 using the four-noded solid thermal elements viz. PLANE55. This element is compatible with the 4-noded structural solid element used in the thermomechanical analysis. This means that the results of the thermal analysis can be successfully exported to perform the thermomechanical analysis.

### 6.4.2 Calculation of Heat Flux

The heat flux applied depends on the contact forces, coefficient of friction and the linear velocity. The total heat generated is calculated by the following simple equation

$$Q = fPv \tag{6.4}$$

where

$f$ = Coefficient of friction

$P$ = Contact force, N

$v$ = Relative velocity, m/s

The heat flux applied is the heat generated applied on the area of contact and is calculated as

$$q_p = \frac{Q}{R * L * \theta_c} \tag{6.5}$$

where

$R$ = Radius of the pin, m

$L$ = Length of the bushing in the normal direction, m

$\theta_c$ = Contact Angle, in radians

### 6.4.3 Implementation of Oscillating Heat Flux

The finite element modeling of the oscillating heat source requires a special formulation. The modeling is done by applying the heat flux as a function of time and space.

The time taken for 1 complete oscillation ($t_{osc}$) is calculated from the speed of oscillation, the angle of oscillation and the radius of the shaft. The calculated time for a single oscillation is broken up into a series of 13 time-steps. The calculated flux is applied over a set of 6 elements in the mean position, Figure 6.2 (a) and then it is solved for the 1 time step i.e. $t_{osc}/13$. For the next time sub-step, the flux is moved to the next set of six elements and then solved again for $2$x($t_{osc}/13$). This solution is appended to the previous solution. The process is continued until a full oscillation is completed. This sequence is programmed into a ANSYS macro (sub-routine) and repeated cyclically to complete the transient analysis.

The application of the flux for 1 cycle is illustrated in Figure 6.3

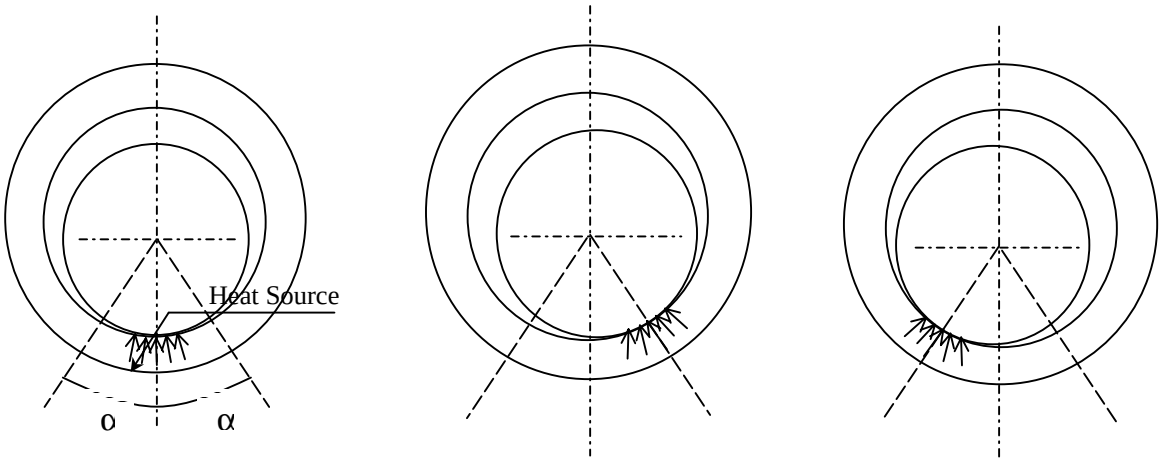


(a) Mean Position (b) Extreme right - +α (c) Extreme left - -α

Figure 6.2 Schematic of application of oscillating flux, $\alpha$ is the oscillation angle

**Sample Calculation of Time for 1 Oscillation**

An example of calculation will now be presented for a bushing operating at a surface velocity of 0.08 m/s with a stationary pin of radius 0.05 m.

$$\Rightarrow \quad \text{Angular velocity, } \omega = \frac{v}{R} = \frac{0.08}{0.05} = 1.6 \textit{radians}/\sec = 91.67 \textit{ degrees/sec}$$

The element size used in the finite element model has an angle of $4.5^{o}$. The theoretical Hertzian contact angle, using Equation 6., is found to be $26.12^{o}$. This means that the flux should be applied over 6 elements.

At the angular velocity of 1.6 rad/s, the time taken for application of flux over a patch of 6 elements before moving to the next set of elements is 0.05 seconds and the flux is applied and solved for every sub-step as illustrated in Figure 6.3. The time taken to negotiate one oscillation ($t_{osc}$) is found to be 0.65 seconds.

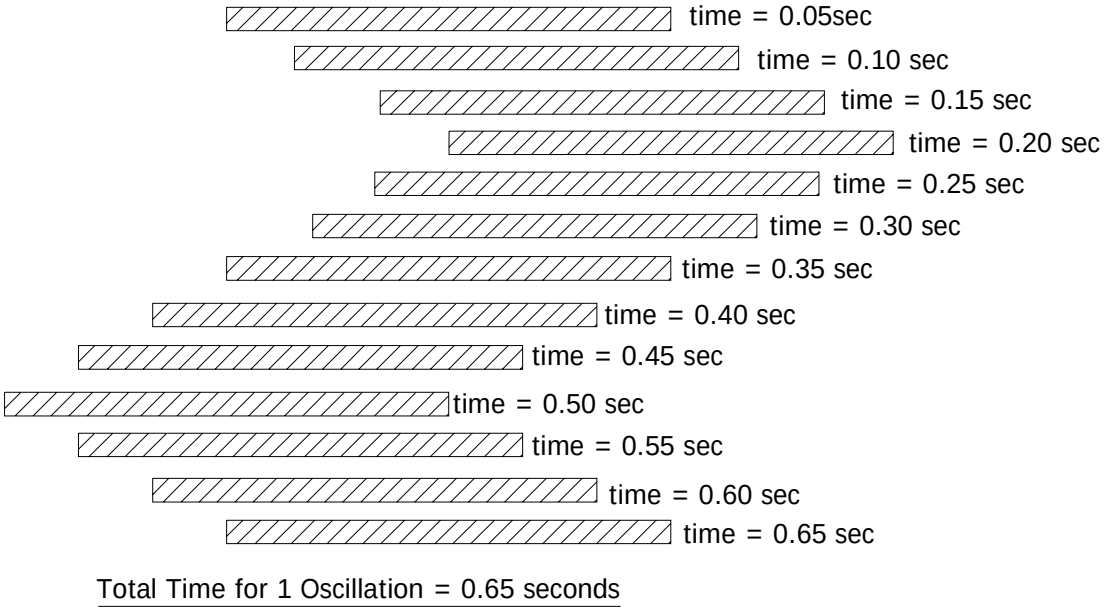


Figure 6.3 –Application of oscillating heat flux as a function of time and space

### 6.4.4 Convection Film Transfer Coefficient between Bushing Outer Radius and Atmosphere

The forced convection coefficient can be theoretically calculated by the empirical relation, Equation 6.6 suggested by A.F. Mills [26] for a cylinder rotating in a fluid. This formula is applicable for a cylinder rotating in an infinite quiescent fluid medium.

$$Nu_D = 0.133\, Re_D^{2/3}\, Pr^{1/3} \qquad (6.6)$$

where the dimensionless numbers are,

$Nu_D$ = Nusselt Number, $hD/k$

$Re_D$ = Reynolds number, $\omega D^2/\nu_k$

$Pr$ = Pradtl Number (0.69 for air)

where,

$h$ = Convective heat transfer coefficient, $W/m^2K$

$D$ = Diameter of the surface on which convection takes place, m

$k$ = Thermal Conductivity of the convecting fluid, W/mK

$\omega$ = Angular velocity of the rotating member, $s^{-1}$

$\nu_k$ = Kinematic viscosity of the convecting fluid, $m^2/s$

The convection between the bushing outer boundary and the environment was found by assuming a mild flow of air over the bushing surface at a speed of 5 mph at a temperature of 300 K. The following parameters are used to calculate the convection HT coefficient.

Convecting Fluid = Air – Properties are obtained from [18]

Temperature of Fluid = 300 K (Room Temperature)

Radius of Bushing = 0.1 m

Velocity of Air = 5 mph (assumed)

**Verification**

The validity of the above method was verified by applying the formula to find the convection coefficient of an axle and cone problem solved by Wang et.al [11]. The convection coefficient calculated using Equation (6.6) was 46 $W/m^2K$ (Appendix). This value was close to the value used by the authors (45 $W/m^2K$) in their analysis.

### 6.4.5. Convective Coefficient in the Gap between Pin and Bushing

The convective heat transfer coefficient in the gap between the pin and bushing needs to be examined in more detail as the temperature rise in the interface between the pin and bushing is high. The high temperature difference between the pin and bushing would contribute to radiation heat transfer between the hot pin and its bushing, which is at a lower temperature. The radiation heat transfer in the analysis by using the concept of linearized radiation coefficient, $h_{rad}$. The total heat transfer coefficient in the gap between pin and bushing thus consists of 2 components.

(i) Forced convective heat transfer coefficient, $h_{forced}$ and

(ii) Equivalent convective heat transfer coefficient $h_{rad}$

The total convective heat transfer coefficient is a summation of the forced convection term and the equivalent radiation term.

$$h_{total} = h_{forced} + h_{rad} \tag{6.7}$$

**Calculation of Forced Convection Coefficient inside the Pin-Bushing Assembly**

The forced convection of air inside the pin-bushing assembly is evaluated using the empirical relation (6.6) using the operating conditions given below. The fluid properties of air are varied to include the entire temperature range that can be expected for various operating conditions.

Convecting Fluid = Air - Properties from Incropera and Dewitt [18]

Temperature of Fluid = 300 K (Room Temperature) - 1100 K (Steady State)

A sensitivity study was done by calculating the forced convection heat transfer coefficient ($h_{forced}$) at various temperature values and it was found that the increase in temperature did not have a significant effect in the temperature range of room

temperature to steady state temperature (about 1100 K). The average forced convective heat transfer coefficient of the sensitivity study was found to be 10 $W/m^2K$ for the temperature range of 300 K – 1100 K.

**Calculation of Equivalent Convective Coefficient due to Radiation**

Steady state thermal analyses for various operating conditions reveal that interface temperatures are in the range of 600 K – 1100 K. These high temperature values can influence the thermal analysis due to heat transfer by radiation between the hot body and the colder body. The heat transfer due to radiation is given by Equation (6.8) [18]

$$q_{rad} = \varepsilon\sigma(T^4 - T_{surf}^4) \tag{6.8}$$

where, $q_{rad}$ = Heat transfer due to radiation, $W/m^2$

$\varepsilon$ = Emissivity of the radiating body

$\sigma$ = Stefan-Boltzmann's constant

$T$ = Surface Temperature of the hotter body, K

$T_{surf}$ = Surface Temperature of the cooler body, $^oK$

The above equation can be rewritten as

$$q_{rad} = \varepsilon\sigma(T^2 + T_{surf}^2)(T + T_{surf})(T - T_{surf}) \tag{6.9}$$

The above equation can be put in the form of a simple convection heat transfer type equation by summing the terms together to be written as an equivalent convective coefficient due to radiation.

$$q_{rad} = h_{rad}(T - T_{surf}) \tag{6.10}$$

where, $h_{rad}$ is the equivalent convective coefficient due to radiation expressed as,

$$h_{rad} = \varepsilon\sigma(T^2 + T_{surf}^2)(T + T_{surf})$$

The equivalent convective coefficient due to radiation varies with the temperature. The heat transfer due to radiation is insignificant when the surface temperatures are very low. Also the heat transfer due to radiation is predominant in the clearance between the pin and bushing and it is not significant on the outer surface of the bushing. So, the equivalent convective coefficient due to radiation, $h_{rad}$ is used along with the regular convective coefficient in the pin-bushing clearance. The variation of $h_{rad}$ with time is linear. The value $h_{rad}$ is calculated by taking the average temperatures on the surface of the pin and the bushing.

### 6.4.6 Boundary conditions for the Thermal Analysis

Heat Flux Applied on the pin, $q_p$= Calculated for different load conditions using Equation 6.5.

Temperatures on the pin and the bushing are coupled in the contact region to achieve continuity of temperature in the contact zone.

Convective HT coefficient

| | | |
|---|---|---|
| On the Bushing outer edges | = | 30 W/m$^2$K |
| In the Pin-Bushing clearance | = | $h_{forced} + h_{rad}$ |
| Average $h_{forced}$ | = | 10 W/m$^2$K |
| Equivalent $h_{rad}$ | = | Linear function of temperature |

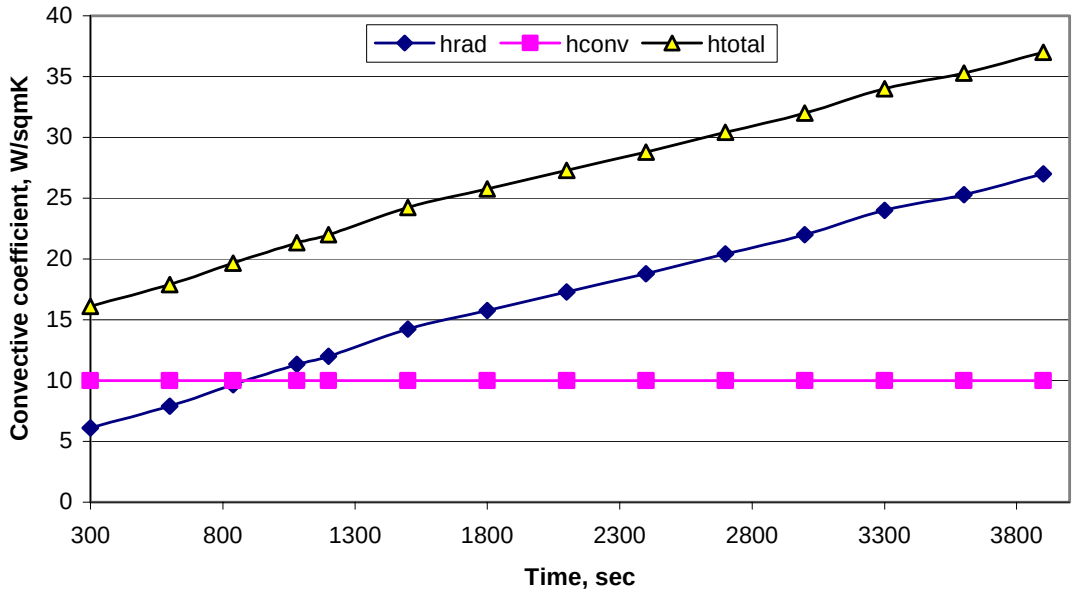


Figure 6.4 – Variation of effective convective coefficient with time

## 6.5 Transient Thermomechanical Analysis

### 6.5.1. Element Types

The solid element PLANE42 is used to model the pin and the bushing. This element is a 2D bilinear element with the x and y displacements as the degrees of freedom and the temperatures obtained from the transient thermal analysis can be applied as nodal loads.

The radial clearance between the pin and the bushing is a problem that has to be dealt with care. The gap is modeled using 2-noded contact elements CONTAC52. Contact elements are used to model gap and they come into effect only when the two nodes that make the element come into contact. The element properties include a normal stiffness value that governs the resistance to normal load. The finite element programmer assigns the stiffness value for the contact element. To determine the stiffness value, the theoretical Hertzian contact width is found. The stiffness value is then fixed at a value by

trial and error so that the Hertzian contact width and the contact width found by Finite Element method are the same. The verification of the stiffness value against the Hertzian theory is a good way to establish validity.

### 6.5.2 Meshing

The meshing pattern is scaled such that the element size is reduced in the radial direction towards the bushing-pin interface. This is done by having coarser elements at the center of the pin and finer elements at the interface. This means that the elements towards the center of the pin degenerate from the standard 4 noded rectangular element into triangles. This methodology is adopted, as our area of interest is the interface of the pin and bushing

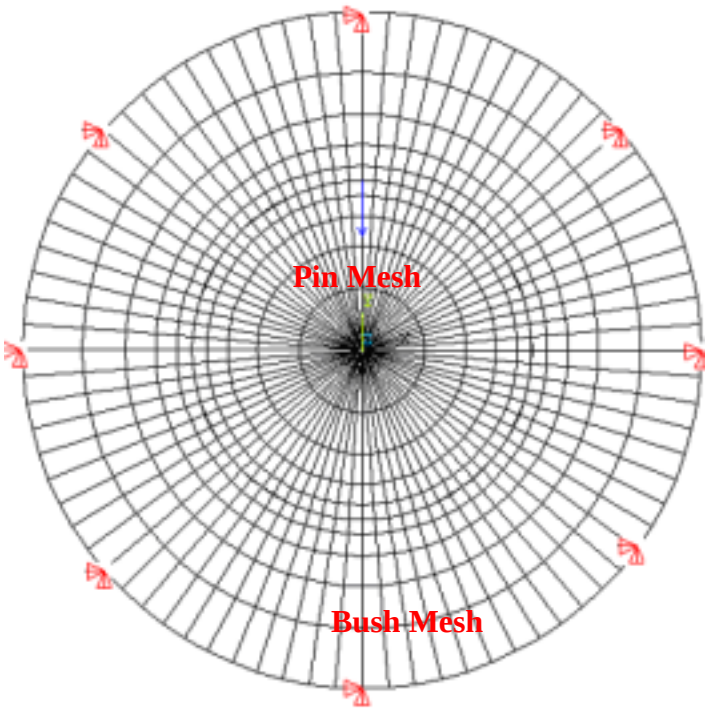


Figure 6.5 – Mesh pattern for the oscillating pin-bushing assembly

### 6.5.3 Boundary Conditions

The radial load is applied on the pin on the centerline and the bushing is constrained on the outer diameter. All the degrees of freedom are constrained. The steady

state analysis is performed and the contact element results are analyzed. The contact element CONTAC52 can display the contact forces and the value of clearance in the gap. The contact element is activated only when there is a physical contact between the pin and the bushing. Whenever there is contact established between the pin and bushing, the contact element results give us the magnitude of the contact force and negative clearance. The stiffness value of the contact element is adjusted such that the contact angle is in agreement with the Hertzian contact angle.

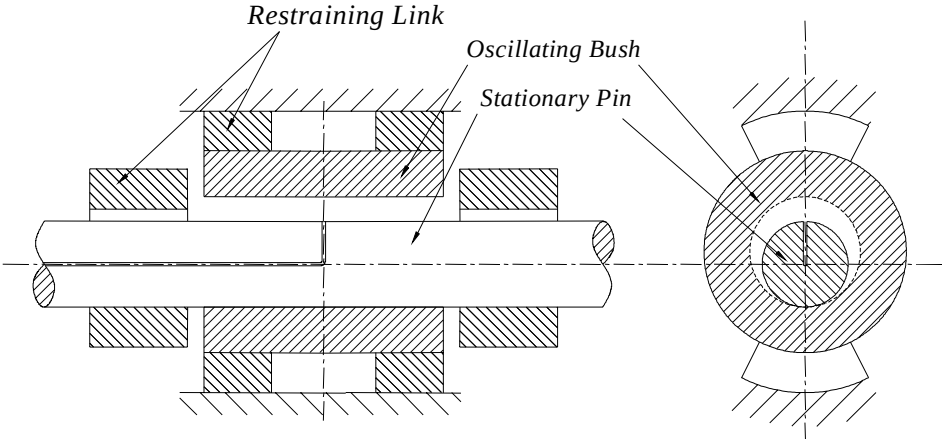


Figure 6.6 – Schematic of a Retention track assembly

The transient thermal analysis is followed by a transient thermomechanical analysis to determine the effects of temperature rise on the operating parameters such as operating clearance and the frictional torque. The results of the thermal analysis are applied as thermal nodal loads with respect to time. The radial load acting on the pin is applied as a point force acting on the centerline.

### 6.6. Operating Parameters

Table 1 – Operating parameters for the finite element model and simulations

| | |
|---|---|
| Range of pin radii, $R_s$ (m) | $35 \times 10^{-3}$ - $75 \times 10^{-3}$ |
| Range of bearing lengths, $L$ (m) | $50 \times 10^{-3}$ - $167 \times 10^{-3}$ |
| Range of radial clearances, $C$ (m) | $0.1 \times 10^{-3}$ - $0.35 \times 10^{-3}$ |

| | |
|---|---|
| Density of pin-bushing $\rho$ (kg/m$^3$) | 1.23 x 10$^6$ |
| Conductivity, $k$ (W/mK) | 54 |
| Thermal expansion coefficient, $\alpha$ (m/mK) | 1 x 10$^{-5}$ |
| Young's modulus of pin-bushing, $E$ (GPa) | 200 |
| Poisson's ratio, $\nu_s = \nu_b = \nu$ | 0.3 |
| Range of loads, $W$ (kN) | 66.723- 222.411 |
| Range of friction coefficient, $f$ | 0.1 – 0.3 |
| Range of oscillating frequencies, $\omega_o$ (rad/s) | 1 - 2 |
| Atmospheric Temperature, $T_\infty$ (°C) | 25 |

**6.7 Results and Discussion**

Simulations are performed for a wide range of operating parameters, while one of the test cases is presented in this section for discussion. Simulations of failure of an oscillating pin-bushing corresponding to the following operating conditions are presented.

| | |
|---|---|
| Pin radius, $R_s$ (m) | 0.05 |
| Bearing length, $L$ (m) | 0.1 |
| Radial clearance, $C$ (m) | 0.25 x 10$^{-3}$ |
| Coefficient of friction, $f$ | 0.3 |
| Oscillating frequency, $\omega_o$ (rad/s) | 2 |
| Load, $W$ (N) | 11205 |

The heat flux as discussed earlier is applied as an oscillating flux with respect to time on the contact region. The oscillating heat flux produces a temperature field as shown in Figure 6.7.

Figure 6.7 gives the temperature profile for the first complete oscillation. The temperature profile for the first four time steps shows the effect of flux moving from the mean position to the extreme right position. The maximum temperature also can be seen to move along in the direction of the moving flux. Time steps 4 through 10 give the temperature profile when the heat flux moves from the extreme right position (+$\alpha$ in

Figure 6.2) to the extreme left position (-α in Figure 6.2). When the flux moves from the extreme right position (Time step #4), it leaves a temperature tail that trails off at the extreme right position (+α).

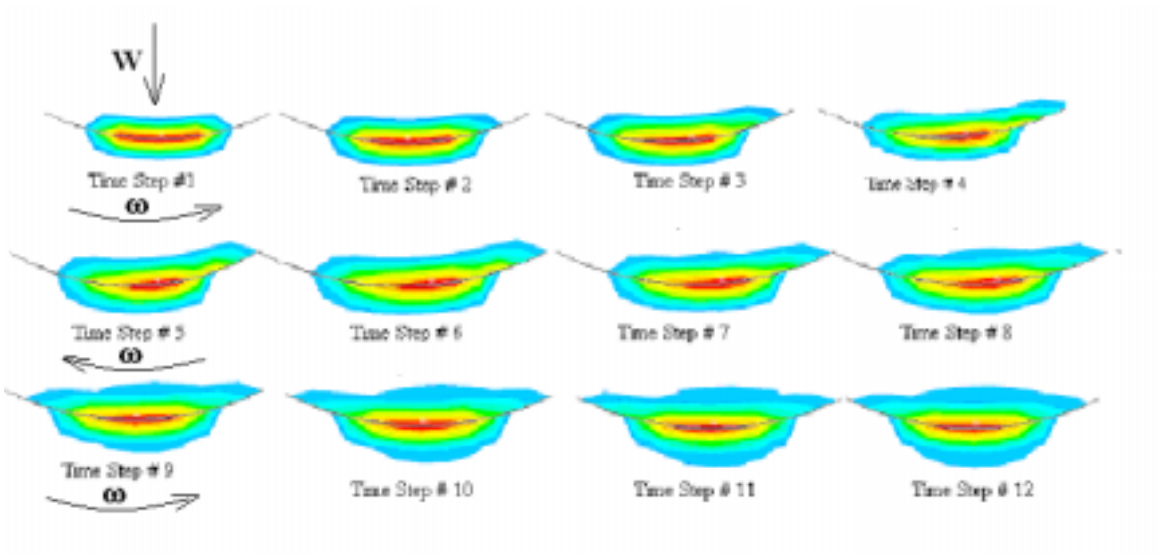


Figure 6.7 – Temperature contour during 1 cycle of oscillation

The temperature rise due to the frictional heating causes thermal expansion of the pin and concomitant reduction in operating clearance. The loss in clearance causes the pin to ovalize and come into contact with the bushing at the top of the shaft. This leads to increased area of contact and increased contact forces. As a result, the frictional heat further contributes to the process of expansion. The temperature profiles are given in Figures 6.8 through 6.11. From the contour profiles, it can be seen that the temperature increases to 752$^{o}$C after about 6 seconds once ovalization is established. This temperature is sufficient to cause scuffing in steel [2]. Also the frictional torque increased to very high values 6 seconds after ovalization was established. Thus the failure can be attributed to both TIS and thermal galling.

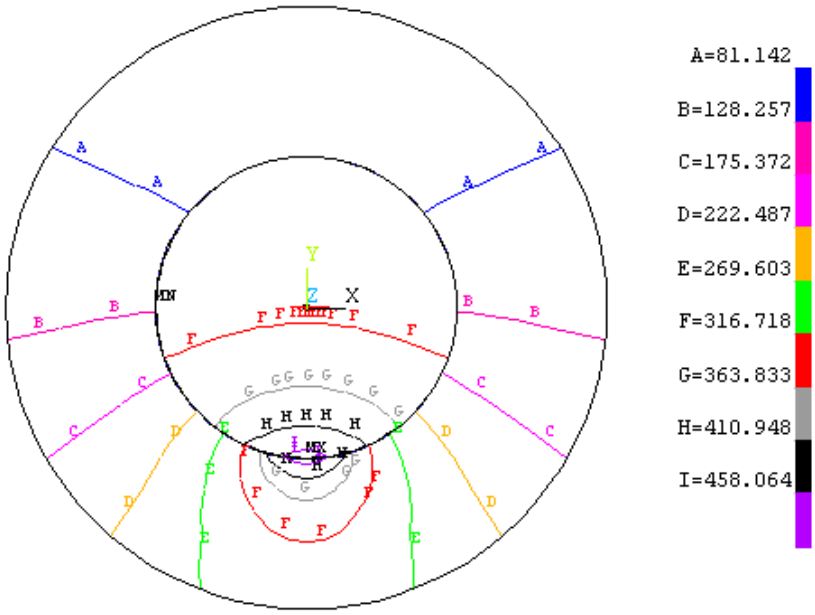


Figure 6.8 – Temperature contour just before ovalization

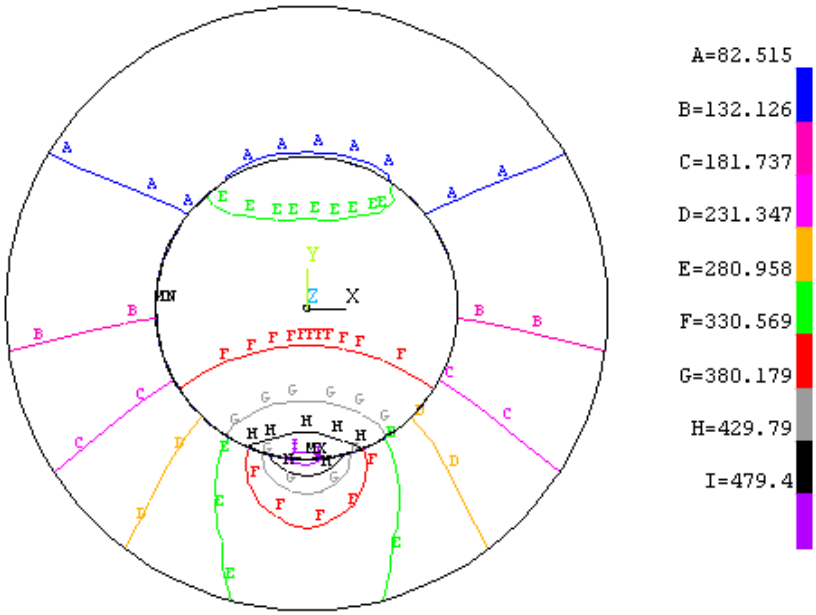


Figure 6.9 – Temperature contour 1 second after initialization of ovalization

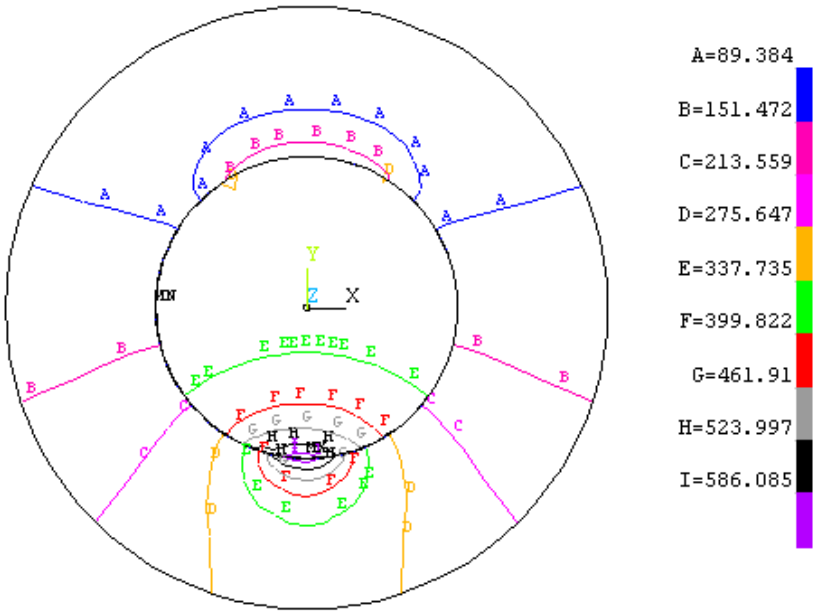


Figure 6.10 – Temperature contour 3 seconds after initialization of ovalization

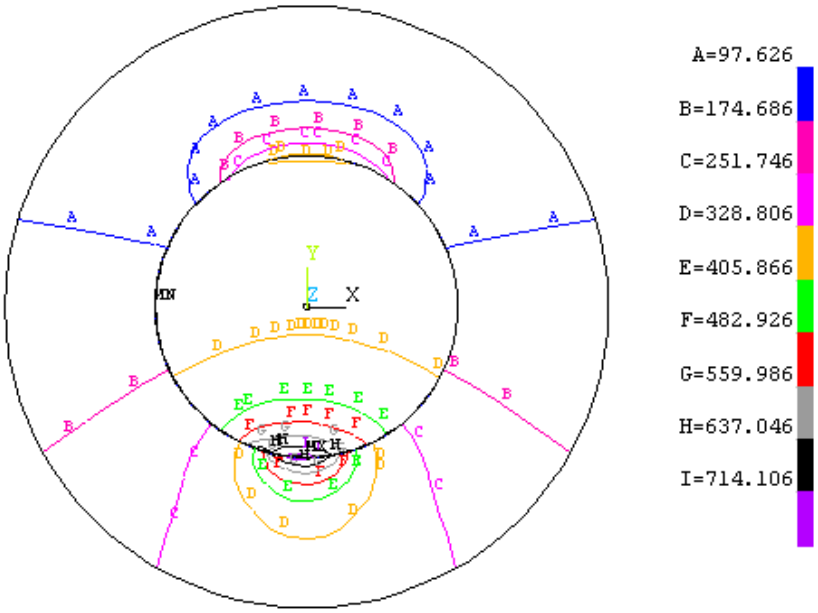


Figure 6.11 – Temperature contour 6 seconds after initialization of ovalization

Note: The maximum temperature at the contact reached 752 $^{o}$C in Figure 6.11 when galling takes place.

The failure pattern is not typically like the example shown in Figures 6.8 to 6.11. The failure mode has a combined mode of thermally induced seizure (TIS) and thermal galling only in very heavily loaded pin-bushing assemblies and where the coefficient of friction and/or the oscillating frequencies are high. In cases were friction coefficients were low, the maximum temperature reached was about 300-400 $^{o}$C and failure occurred by thermally induced seizure (TIS). Typically lightly loaded assemblies with low coefficients of friction failed by TIS mode while the heavily loaded assemblies and when the coefficients of friction were higher, a combination of thermal galling and TIS was observed within the range of simulations performed.

**6.8 Generalization**

A number of simulations (Table 6.2) were performed to study and derive a generalized equation to determine the time of failure of an oscillating pin-bushing assembly. Non-dimensional parameters were used to generalize the operating parameters. The non-dimensional parameters used in this analysis are similar to the non-dimensional parameters used in Chapter 4 in the study of TIS in journal bearings during start-up and are given below.

Non-dimensional seizure time: $$\bar{t}_{fo} = \frac{t_{fo}\kappa}{R_s^{\,2}}$$

Thermal strain: $$\varepsilon = \frac{fW\omega_o\alpha}{k_s}$$

Modified aspect ratio: $$\lambda = \frac{R_{eq}}{L} \text{ , where } R_{eq} = \frac{R_s R_{bi}}{R_{bi} - R_s} = \frac{R_s(R_s + C)}{C}$$

Table 6.2 – Variation of failure time at various operating conditions

| *Coefficient of friction, f* | *Angular velocity, $\omega_o$,* (rad/s) | *Load, W* (kN) | *Pin Radius, $R_p$,* (mm) | *Clearance, C* (mm) | *Length,L* (mm) | *Failure time, $t_{fo}$ (s)* | *Thermal Strain,$\varepsilon$* | *Aspect Ratio,$\lambda$* | *Non-dimensional time for failure, $t_{fo}$* | *Temperature at Failure, ($^oC$)* |
|---|---|---|---|---|---|---|---|---|---|---|
| 0.1 | 1 | 111.21 | 50 | 0.25 | 100 | 6053 | $2.139 \times 10^{-03}$ | 100.5 | 37.19 | 300 |
| 0.1 | 1.6 | | | | | 2535 | $3.422 \times 10^{-03}$ | | 15.58 | 322 |
| 0.15 | 1.2 | | | | | 2399 | $3.849 \times 10^{-03}$ | | 14.74 | 343 |
| 0.2 | 1.4 | | | | | 1488 | $5.988 \times 10^{-03}$ | | 9.143 | 374 |
| 0.2 | 1.5 | | | | | 1207 | $6.416 \times 10^{-03}$ | | 7.416 | 380 |
| 0.25 | 1.6 | | | | | 936 | $8.554 \times 10^{-03}$ | | 5.75 | 417 |
| 0.27 | 1.8 | | | | | 749 | $10.97 \times 10^{-03}$ | | 4.602 | 442 |
| 0.3 | 2 | | | | | 582 | $12.83 \times 10^{-03}$ | | 3.58 | 492 |
| 0.2 | 1.5 | 66.72 | | | | 3018 | $3.849 \times 10^{-03}$ | | 18.544 | 329 |
| | | 222.42 | | | | 564 | $12.83 \times 10^{-03}$ | | 3.47 | 461 |
| | | | | | | | | | | |
| 0.2 | 1.5 | 111205 | 50 | 0.1 | 100 | 322 | $6.416 \times 10^{-03}$ | 250.5 | 1.98 | 205 |
| | | | | 0.15 | | 604 | | 167.17 | 3.71 | 265 |
| | | | | 0.2 | | 1006 | | 125.5 | 6.18 | 314 |
| | | | | 0.25 | | 1207 | | 100.5 | 7.42 | 380 |
| | | | | 0.3 | | 1408 | | 83.83 | 8.65 | 440 |
| | | | | 0.35 | | 2532 | | 71.93 | 15.56 | 465 |
| | | | 35 | 0.25 | | 2380 | | 49.35 | 29.84 | 405 |
| | | | 75 | | | 805 | | 225.75 | 2.20 | 446 |
| | | | 50 | | 50 | 564 | | 201 | 3.47 | 461 |
| | | | | | 100 | 1207 | | 100.5 | 7.42 | 380 |
| | | | | | 166.67 | 2938 | | 60.3 | 18.05 | 325 |

The number of simulations is reduced by just varying the non-dimensional parameters instead of varying all the operating parameters making sure that the physical significance of the operating parameters is not lost. The effect of various operating parameters like load ($W$), coefficient of friction ($f$) and frequency of oscillation ($\omega_b$) on the failure time is found by varying the non-dimensional parameter $\varepsilon$. The number of simulations required is thus greatly reduced. The results of varying the various operating parameters are given in Table 6.1.

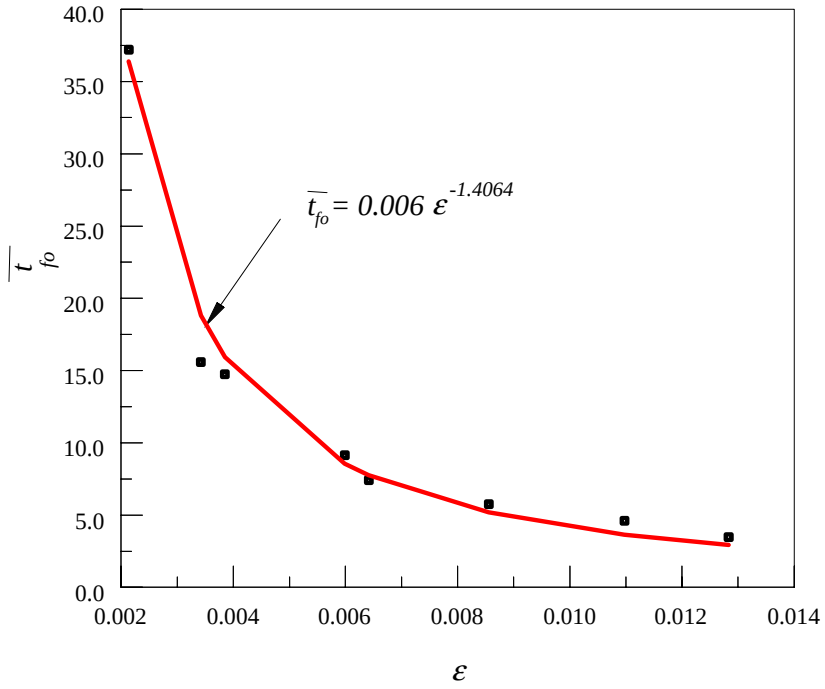


Figure 6.12 – Thermal Strain vs non-dimensional failure time

The results presented in Table 6.1 were curve fitted to a goodness value within 98.9% as shown in Figures 6.12 and 6.13. The expressions relating the thermal strain, aspect ratio and non-dimensional failure time were combined to give the following equation 6.11 for failure time for pin-bushing that undergo failure under oscillating boundary conditions.

$$\overline{t_{fo}} = \frac{\varepsilon^{-1.4064}}{2.255\lambda - 70.71} \tag{6.11}$$

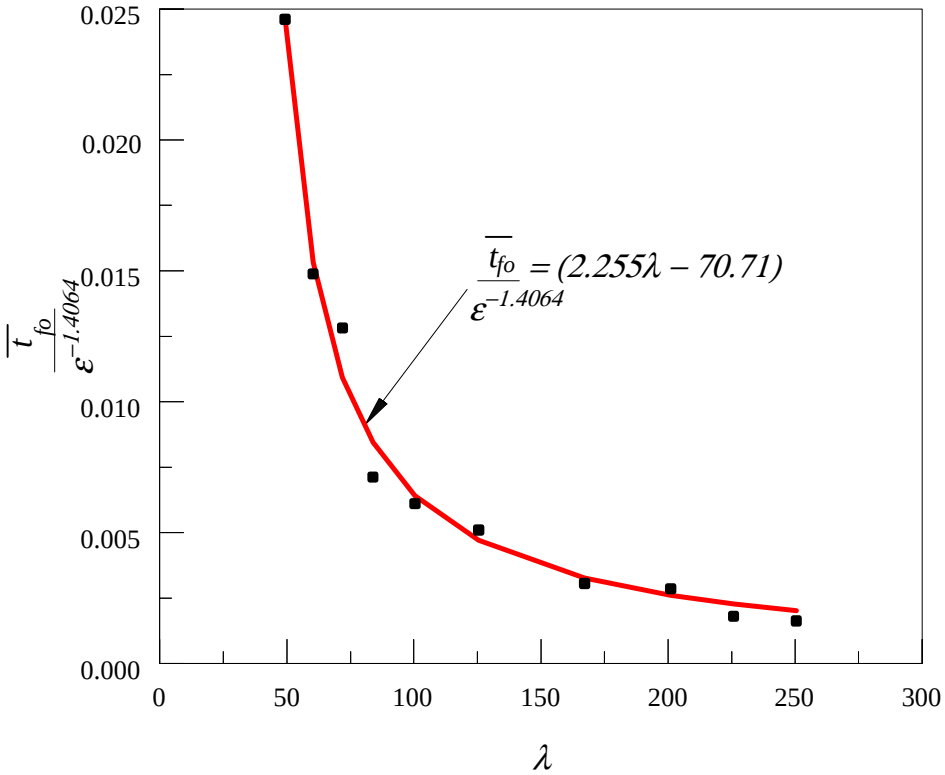


Figure 6.13 – Variation of aspect ratio with non-dimensional seizure time

**6.9 Verification**

The primary reason for failure in the analysis of the pin-bushing assembly is due to the increase in temperature due to frictional heating. The application of proper boundary conditions for the thermal analysis has to be verified to ensure accuracy of the model. A comparison was done between the heat conduction finite element problem done using ANSYS for a one domain problem with the oscillating heat source applied on the pin. Krishnamurthy and Khonsari [27] verified the accuracy of the finite element model by applying Duhamel's theorem to problems involving oscillating heat source. They also performed dimensional and non-dimensional analysis using another FE solver, FlexPDE [24]. The results of the finite element problems solved using ANSYS and FlexPDE

matched closely with the analytical solution. The convergence of the finite element model was also checked using three different mesh sizes.

### 6.10 Restrictions and Applications

(i) The finite element was solved by approximating it as a 2-dimensional problem, assuming that the contact pressure is uniform across the bearing length and there is no misalignment of the shaft in the bearing. The material properties were assumed to be constant and the analysis did not consider plastic deformation.

(ii) The time for failure as given in Equation (6.11) gives the approximate failure time ($t_{fo}$) after there is complete loss of initial lubrication in the pin-bush assembly and loss of anti-friction coating.

(iii) Equation (6.11) gives the failure time for pin-bush assembly when there is continuous oscillating motion. But in practice, there is only intermittent loads acting on the pin-bushing assembly. The time to failure predicted is for the worst-case scenarios. To obtain a practical failure time, the loading cycle of the oscillating pin-bushing has to be incorporated with Equation (6.11).

(iv) The Hertzian contact pressure in the contact region is elliptic and hence the frictional heat flux is also elliptic. But a constant heat flux is applied in the thermal analysis.

(v) The oscillating frequency, $\omega_b$, is assumed to be constant for small intervals of time.

# CHAPTER 7. CONCLUSIONS

## 7.1 TIS in Journal Bearings During Start Up

When rotating machinery that is supported on fully lubricated bearings are started up from rest, the lubrication flow may not have been established and there would be metal-to-metal contact. The effect of the dry sliding during start-up was analyzed by studying the effect of start-up friction on the bearing operating parameters such as clearance loss and frictional torque by a thermoelastic finite element model.

A series of simulations were performed by varying the operating parameters. A statistical analysis was performed using the simulated results to determine the relationship of these operating parameters on the seizure time. An empirical relationship was developed to estimate the seizure time using these operating parameters. The procedure for applying the empirical relation and the interpretation of results that can be deduced from the empirical relation is described. The restrictions involved in using the empirical relation are also specified. The accuracy of the empirical relation was verified using published results. The final expression for the seizure time is given by the following equations

$$\overline{t_s} = 90.494\, \varepsilon^{-1.2478}\, \lambda^{-1.6494} \qquad \text{For } 500 < R_s/C < 1000$$

$$\overline{t_s} = 1.825\, \varepsilon^{-1.2478}\, \lambda^{-1.02718} \qquad \text{For } 1000 < R_s/C < 5100$$

## 7.2 TIS in Journal Bearings During Transient Flow Disturbance

The sudden stoppage in the lubricant flow, in a fully flooded journal bearing was analyzed. The interruption in the lubricant flow was modeled in finite element analysis by an increase in the coefficient of friction and a decrease in the convective cooling. The effect of the lubricant cut-off was analyzed by studying its effect on the bearing operating parameters such as clearance loss and frictional torque by a thermoelastic finite element

model. An expression relating the seizure time to the operating parameters for a journal bearing undergoing a transient flow disturbance was derived in the same procedure as explained for the case of TIS during start up. The empirical relationships relating seizure time to operating parameters when a flow disturbance is encountered are given by the following equation.

$$\overline{t_{sp}} = \left(\varepsilon^{\,0.5489}\left(0.0065\lambda + 9.314\right)\right)^{-1}$$

### 7.3 TIS and Thermal Galling in Oscillating Pin-Bushing Analysis

The analysis of a heavily loaded pin-bushing assembly subject to oscillating loading was analyzed using finite element thermal analysis and thermomechanical analysis. The reasons for bearing failure were analyzed by performing simulations for different types of operating conditions. It was found that failure of these pin-bushings occurred by thermally induced seizure for lighter boundary conditions and by a combination of TIS and thermal galling for more severe boundary conditions. The time for failure in the non-dimensional form was derived from a series of simulations and is given by the following equation.

$$\overline{t_{fo}} = \frac{\varepsilon^{-1.4064}}{2.255\lambda - 70.71}$$

## BIBLIOGRAPHY


1. **Ling F. F. and Saibel E.** Thermal aspects of galling of dry metallic surfaces in sliding contact. *Wear, 1958*, **1**, 80-91

2. **Dyson A.** Scuffing. *Treatise on Material Science and Technology, 1979*, **13**, 175-215

3. **Gecim B. and Winer W. O.** Steady State Temperature in a Rolling Cylinder Subject to Surface Heating and Convective Cooling. *ASME Journal of Tribology, 1984*, **106**, 120-127

4. **Patula E. H.** Steady State temperature Distribution in a Rotating Roll Subject to Surface Heat Fluxes and Convective Cooling. *ASME Journal of Tribology, 1981*, **103**, 36-41

5. **Ulysee P. and Khonsari M. M.** Thermal Response of Rolling Components Under Mixed Boundary Conditions: An Analytical Approach, ASME Journal of Heat Transfer, 1993, **115**, 857-865

6. **Bishop J.L. and McC. Ettles C.M.** The seizure of journal bearings by thermoelastic mechanisms. *Wear, 1982*, **79**, 37-52

7. **Dufrane K. and Kannel J.** Thermally induced seizures of journal bearings. *ASME Journal of Tribology*, 1989, **111**, 288-92

8. **Khonsari M.M. and Kim H.J.** On thermally induced seizure in journal bearings. *ASME Journal of Tribology*, 1989, **111**, 661-7

9. **Hazlett T.L. and Khonsari M.M**. Finite element model of journal bearing undergoing rapid thermally induced seizure. *Tribology International*, 1992a, **25**, 177-82

10. **Hazlett T.L.** Thermoelastic behavior of journal bearing undergoing seizure – a finite element study. *M.S. Thesis, University of Pittsburgh, Pittsburgh, Pennsylvania, 1990*

11. **Wang H., Conry T.F. and Cusano C.** Effects of Cone/Axle Rubbing Due to Roller Bearing Seizure on the Thermomechanical Behavior of a Railroad Axle. *ASME Journal of Tribology*, 1996, Vol.118, pp.311-319

12. **Wang H.,** Axle Burn-off and Stack-up Force Analyses of a Railroad Roller Bearing using the Finite Element Method. *Ph.D. Thesis, Department of Mechanical and Industrial Engineering, University of Illinois at Urbana-Champaign*, 1996, p 35, pp.140-147.

13. **Wang Q.,** Seizure Failure of journal-bearing conformal contacts. *Wear*, 1997, **210**, pp.8-16.

14. **Lacey S. and H. Kawamura H.,** Bearings for Aircraft Gas Turbine Engines (Part 1), *NSK Technical Journal – Motion and Control*, 1998, **5**, pp. 1-8

15. **Pascovici M.D., Khonsari M.M. and Jang J.Y.,** On the Modeling of Thermomechanical Seizure. *ASME Journal of Tribology*, 1995, **117**, 744-7

16. **Jang J.Y., Khonsari M.M. and Pascovici M.D.,** Thermohydrodynamic Seizure: Experimental and Theoretical Analysis. *ASME Journal of Tribology*, 1998, **120**, 8-15

17. **Cook R.D., Malkus D.S. and Plesha M. E.**, Concepts and Applications of Finite Element Analysis, *John Wiley and Sons, 1989, Third Edition*

18. **Incropera F.P. and Dewitt D. P.** Fundamentals of Heat and Mass Transfer, *John Wiley and Sons, 1996, Fourth Edition*

19. ANSYS 5.7 Online Users Manual, 2001, *ANSYS Inc*

20. **Peterson M.B. and Winer W.O.** Wear Control Handbook, *ASME*, 1980, 115

21. **Hamrock B.J.** Elastohydrodynamic lubrication of point contacts. *Ph.D Thesis, Institute of Tribology, Department of Mechanical Engineering, The University of Leeds*, 1976, 44-66, pp. 93-102

22. **Khonsari M.M., Booser E.R.,** Applied Tribology, *John Wiley and Sons Inc.*, 2001

23. **Bolz R. E., Tuve T.L.,** CRC Handbook of Tables for Applied Engineering Science, *CRC Press*, Second Edition, 1970, p 621, pp 117-19, pp 153-155

24. **Khonsari M.M. and Kim H.J.**, Discussion on paper titled "Thermally induced seizures of journal bearings" by Dufrane K. and Kannel J., *ASME Journal of Tribology*, 1989, **111**, 292

*25.* FlexPDE: A Flexible Solution for Partial Differential Equations Version 2.20e 3D Online Reference Manuals, 1996-2001, *PDE Solutions Inc*

26. **Mills A.F**., Heat and Mass Transfer, *Richard D Irwin Inc*., 1995

27. **Krishnamurthy H.,** "Application of Duhamel's Theorem to Problems Involving Oscillating Heat Source" *M. S. Thesis, Department of Mech. Engr., LSU, 2002*

## APPENDIX - MAPLE PROGRAM TO CALCULATE CONVECTION COEFFICIENT

The formula to find the convection coefficient of an axle and cone problem solved by Wang et.al [11]. The convection coefficient calculated using Equation (6.6) was 46 W/m$^2$K while Wang et. al. reported the convection coefficient to be 45 W/m$^2$K for the operating conditions reported below.

Train speed = 55 mph;
Axle rotating speed = 560 rpm
Ambient air temperature = 25 $^o$C
Shaft radius = 78.632 mm

**Maple Program:**

```
> restart;
> with(linalg):
Warning, the protected names norm and trace have been redefined and
unprotected
```

```
> Nusselt[forced] := 0.133*Reynolds^(2/3)*Pr^(1/3);
```

$$Nusselt_{forced} := .133\ Reynolds^{(2/3)}\ Pr^{(1/3)}$$

```
> Reynolds := omega*Dia^2/nu;
```

$$Reynolds := \frac{\omega\ Dia^2}{\nu}$$

```
>
> omega := V/R;
```

$$\omega := \frac{V}{R}$$

**Free Convection coefficient from Incropera and Dewitt**

```
> Nusselt[free] := (0.60 +
0.387*Ra^(1/6)/(1+(0.559/Pr)^(9/16))^(8/27))^2;
```

$$Nusselt_{free} := \left( .60 + \frac{.387\ Ra^{(1/6)}}{\left(1 + .7209732340 \left(\frac{1}{Pr}\right)^{(9/16)}\right)^{(8/27)}} \right)^2$$

```
> Nusselt[total] := Nusselt[forced] + Nusselt[free];
```

$$Nusselt_{total} := .133\left(\frac{V\,Dia^2}{R\,\nu}\right)^{(2/3)} Pr^{(1/3)} + \left(.60 + \frac{.387\,Ra^{(1/6)}}{\left(1 + .7209732340\left(\frac{1}{Pr}\right)^{(9/16)}\right)^{(8/27)}}\right)^2$$

```
> Ra := g*beta*(T[s]-T[inf])*Dia^3/(nu*alpha);
```

$$Ra := \frac{g\,\beta\,(T_s - T_{inf})\,Dia^3}{\nu\,\alpha}$$

```
> beta := 1/T[inf];
```

$$\beta := \frac{1}{T_{inf}}$$

```
> Dia := 2*R;
```

$$Dia := 2\,R$$

Enter the Kinematic viscosity of the fluid - air

```
> nu := 15.89e-6;
```

$$\nu := .00001589$$

Enter the velocity of the shaft in m/s

```
> V := 4.6112;
```

$$V := 4.6112$$

Enter the radius of the shaft, in meter

```
> R := 0.078632;
```

$$R := .078632$$

Enter the thermal conductivity of the fluid, in SI units

```
> k := 26.3e-3;
```

$$k := .0263$$

Enter the Prandtl Number for the fluid

```
> Pr := 0.69;
```

$$Pr := .69$$

Enter the Acceleration due to gravity value in the proper units;

```
> g := 9.8;
```

$$g := 9.8$$

Enter the Diffusivity of the fluid

```
> alpha := 22.5e-6;
```

$$\alpha := .0000225$$

Enter the Fluid Bulk Temperature (in degree K)

```
> T[inf] := 300;
```

$$T_{inf} := 300$$

Enter the Mean Temperatur rise on the surface of the shaft;

> **T[s] := 373;**

$$T_s := 373$$

> **h := Nusselt[total]*k/Dia;**

$$h := 46.09811930$$

## VITA

Mr. Rajesh Krithivasan was born on February 4, 1976, in Madurai, India. He earned his bachelor's degree in mechanical engineering from Bharathiyar University, India. After his undergraduate studies, he worked as a design engineer in Ashok Leyland Limited, India, for 2 years. He joined Louisiana State University in August 1999 to pursue a master's degree in mechanical engineering. His area of interests include tribology, computer aided designing/manufacturing and finite element methods. He successfully defended his thesis work on October 7, 2002, and will receive the degree of Master of Science in Mechanical Engineering in December 2002.